The *Chandra* view of galaxy mergers

Nicola J. Brassington,[1]⋆ Trevor J. Ponman[1] and Andrew M. Read[2]

[1]*School of Physics and Astronomy, The University of Birmingham, Edgbaston, Birmingham B15 2TT*
[2]*Department of Physics and Astronomy, University of Leicester, University Road, Leicester LE1 7RH*

ABSTRACT

From a *Chandra* survey of nine interacting galaxy systems the evolution of X-ray emission during the merger process has been investigated. It is found that the X-ray luminosity peaks ∼300 Myr before nuclear coalescence, and then dips, even though we know that rapid and increasing activity is still taking place at this time. It is likely that this drop in X-ray luminosity is a consequence of outflows breaking out of the galactic discs of these systems. In this work it is also shown that, for the systems close to the point of nuclear coalescence, L_{FIR} becomes massively enhanced compared to the X-ray luminosity of these systems. We suggest that this enhancement may indicate a 'top heavy' initial mass function (IMF), with an enhanced fraction of massive stars.

At a time ∼1 Gyr after coalescence, the merger remnants in our sample are X-ray faint when compared to typical mature elliptical galaxies. However, we do see evidence that these systems will start to resemble typical elliptical galaxies at a greater dynamical age, given the properties of the 3-Gyr system within our sample, supporting the idea that halo regeneration will take place within low L_X merger remnants.

As a part of this survey, detailed *Chandra* observations for the double nucleus merger system Markarian 266 (Mrk 266) and the merger remnant Arp 222 are presented for the first time. With the Mrk 266 observation, in contrast to previous studies, we now have good spectral information of the individual components part seen with the *ROSAT* High Resolution Imager (HRI). Additionally, the structure of the emission to the north of the system can clearly be distinguished and there is also a suggestion of some extension of X-ray emission to the south-east of the nuclear region, indicating that this galaxy could just be on the verge of large-scale galactic winds breaking out. Within Arp 222 an X-ray luminosity of 1.46×10^{40} erg s^{-1} has been detected, this is the lowest value of L_X within our sample. The diffuse gas of Arp 222 has been modelled with a temperature of 0.6 keV and, from CO observations it has been found to host very little molecular gas, indicating that, from current observations, Arp 222 does not resemble a mature elliptical.

Key words: stars: formation – stars: luminosity function, mass function – ISM: jets and outflows – galaxies: evolution – galaxies: interactions – X-rays: galaxies.

1 INTRODUCTION

It is widely believed that very few galaxies exist today that have not been formed or shaped in some way by an interaction with another galaxy. Toomre (1977) identified 11 galaxies that exhibit characteristics of on-going mergers, and arranged them in a chronological order, illustrating how spiral galaxies can merge to produce ellipticals. It is now the view of many astronomers that this process, whilst not the only mechanism to create these systems, plays a vital role in the production of elliptical galaxies. The 11 systems within the 'Toomre' sequence, alongside other examples of on-going mergers, have been studied in great detail over a range of wavelengths to try and characterize exactly how these systems evolve. When studying these merging galaxies, X-ray observations are of particular importance, as they are able to probe the dusty nucleus of the system, which can be obscured at other wavelengths, allowing the nature of the point source population to be established. Furthermore, imaging of the soft X-ray emission permits the diffuse hot gas to be mapped out. This gives important information about the hot gaseous component associated with the strong starburst, and allows galactic winds outflowing from the system to be observed, enabling constraints to be placed on the energetics of these outflows.

⋆E-mail: njb@star.sr.bham.ac.uk

X-ray observations were initially carried out with the *Einstein Observatory*, providing limited spatial resolution. This instrument was followed by *ROSAT*, which greatly improved the sensitivity of the observations, allowing the X-ray properties of these merging galaxies to be probed. A study of a sample of interacting systems was carried out by Read & Ponman (1998, hereafter RP98), where the X-ray luminosity and properties of the diffuse gas were investigated with *ROSAT*, alongside the point source population. In this study it was found that the normalized X-ray luminosity of these systems, broadly speaking, followed the normalized L_{FIR} luminosity, peaking at the time of coalescence. It was also found that the young merger-remnant systems within the sample exhibited low X-ray luminosities, with no indication from the later stage systems in their sample that these systems would increase in X-ray luminosity. However, it was noted that the ~1-Gyr system, NGC 7252, still hosts a large amount of molecular gas, in the form of tails and loops, and given more time to evolve, the X-ray properties could resemble those of a mature elliptical galaxy at a greater dynamical time. The main limitation of this study, due to the *ROSAT* observations, was the inability to disentangle the point sources from the diffuse gas, particularly at larger distances.

With the next generation of X-ray observatories this issue was addressed with an increase in spatial resolution. This improvement, provided by *Chandra*, has allowed the investigation of both the diffuse gas and the point source population of galaxies to be carried out in greater detail. The ability to disentangle these two components is vital when investigating interacting and merging galaxies, as studies have shown that both of these components have different evolutionary time-scales (Read & Ponman 2001). It is therefore important to be able to study both of these separately, to fully understand how they evolve.

From observing a selection of interacting galaxy systems, at different stages of evolution, the processes involved in the merging of galaxies pairs can be characterized. In the following sections we will describe the sample we have selected, and investigate the behaviour of the X-ray emission as the galaxies evolve from two spiral galaxies, through to relaxed merger remnants. Section 2 outlines the selection criteria we have used and gives a brief description of each system. In Section 3 we present the results from new *Chandra* observations of Markarian 266 (Mrk 266) and Arp 222. Correlations and evolution of X-ray emission across the whole sample is presented in Section 4, and discussed in Section 5. Conclusions are given in Section 6.

2 THE SAMPLE

To gain a better understanding of galaxy evolution it is important to compare similar systems that are undergoing the same transformation. By compiling a sample of these galaxies, the evolution of the systems' X-ray properties can be investigated. In this paper we have a sample of nine interacting and post-merger systems, carefully selected to ensure that they are representative of galaxies undergoing a major merger. The nine systems were selected using the following criteria.

(i) All systems have been observed with *Chandra*.
(ii) Systems compose of, or, originate from, two similar mass, gas rich, spiral galaxies.
(iii) Multiwavelength information is available for each system.
(iv) The absorbing column is low, maximizing the sensitivity to soft X-ray emission.

(v) A wide chronological sequence is covered; from detached pairs to merger remnants.

Once the nine systems to study had been selected, the issue of merger age had to be addressed. This is one of the main problems when working with a chronological study such as this, and a number of different methods are required to solve this problem. First, the point of nuclear coalescence was assigned to be at time 0. From this, the time taken until nuclear coalescence for each pre-merger system can then be estimated. These time-scales were derived with a combination of *N*-body simulations, such as Mihos & Hernquist (1996), and dynamical age estimates, where the length and faintness of tidal tails, as well as nuclei separation, were used (Toomre & Toomre 1972). For post-merger systems, assigning an age estimate was done by making the assumption that the last widespread episode of star formation within the system took place at the time of nuclear coalescence. Stellar population synthesis models were then used to calculate these time-scales, therefore, giving a good merger age estimate (Bruzual & Charlot 1993). In the following subsections a brief description of the nine merger examples, and their X-ray properties, are presented in chronological order.

2.1 Arp 270

The earliest example of an interacting system in our sample is Arp 270 (also NGC 3395/3396). This comprises two spiral galaxies of comparable mass (Hernández-Toledo & Puerari 2001), separated by 12 kpc at a distance of 28 Mpc (assuming $H_0 = 75\,\text{km}\,\text{s}^{-1}\,\text{Mpc}^{-1}$, and accounting for Virgocentric in-fall). These galaxies are connected by an optical bridge which is thought to have formed during the systems first perigalactic passage which occurred approximately 5×10^8 yr ago.

A 20-ks *Chandra* observation of the system was made in 2001 and is discussed in detail in Brassington, Read & Ponman (2005), the contours of adaptively smoothed 0.3–8.0 keV X-ray contours overlaid on an optical image are shown in Fig. 1. From this observation 16 point sources are detected, seven of which are classified as ultraluminous X-ray sources (ULXs), with $L_X \geqslant 1 \times 10^{39}\,\text{erg}\,\text{s}^{-1}$ (Soria, Cropper & Motch 2005). The diffuse gas emits at a global temperature of ~0.5 keV and shows no evidence of hot gaseous outflows as are seen in later stage systems (RP98). The galaxy pair, although in a very early stage of interaction, already show increased levels of L_{FIR} compared to quiescent galaxies, indicating that there is enhanced star formation taking place. The numerical simulations of Mihos & Hernquist (1996) suggest that a system such as Arp 270 will coalesce in ~650 Myr.
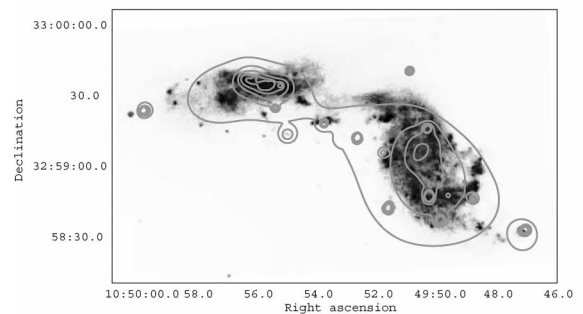

Figure 1. The early merger system Arp 270. Contours of adaptively smoothed 0.3–8.0 keV X-ray data from *Chandra* ACIS-S overlaid on an optical image from the Palomar 5-m telescope.
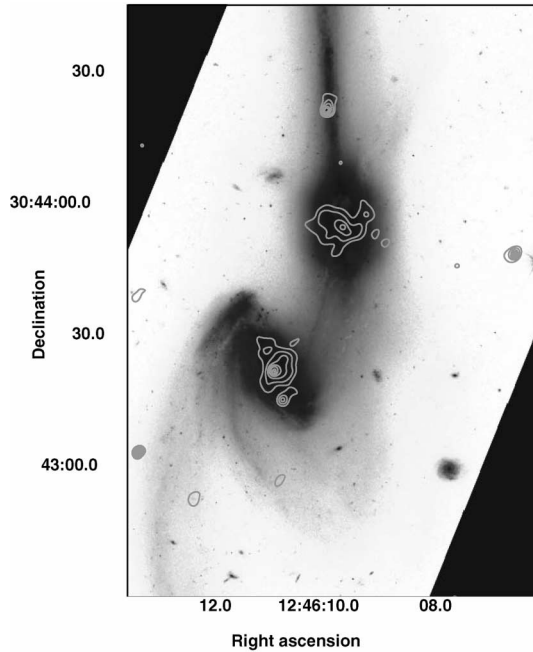
Figure 2. The Mice, contours of adaptively smoothed 0.2–10.0 keV X-ray data from *Chandra* ACIS-S overlaid on an optical image from WFPC2 on board the *HST*.

2.2 The Mice

The Mice (also Arp 242, NGC 4676A/B) is another early stage merger system, lying second in the evolutionary sequence proposed by Toomre & Toomre (1972). At a distance of 88 Mpc, the two detached spiral galaxies are again connected by a tidal bridge and, in addition to this feature, exhibit large tidal tails, a consequence of the galaxies interacting as they have passed each other. Read (2003) reports on a 30.5-ks *Chandra* observation of the system, the adaptively smoothed 0.2–10.0 keV X-ray contours overlaid on an optical image are shown in Fig. 2.

Five ULXs are detected in association with the galaxies, these sources have been found to be coincident with regions of ongoing star formation, both within the nuclei of the galaxies and also in the tidal tails. The structure of the diffuse X-ray gas in both nuclei suggests that this system is at a more advanced stage of evolution than Arp 270. This is indicated by the morphology of the gas, a soft, thermal plasma, which extends out of the minor axis of both galaxies, suggesting that these features are starburst-driven winds. As in Arp 270, the Mice emits an enhanced level of $L_{\rm FIR}$, again indicating that this system has enhanced star formation taking place, this emission is particularly high in the nuclei of the galaxies.

2.3 The Antennae

The Antennae, NGC 4038/4039, or Arp 244, is probably the most famous example of a galaxy pair undergoing a major merger, and, lying at a distance of 19 Mpc, is also the nearest. A deep integrated *Chandra* observation of 411 ks has been made of this system, enabling the nature of both the point source population and the diffuse gas to be investigated (Fabbiano et al. 2004; Zezas et al. 2006), Fig. 3 shows the full band (0.3–6.0 keV) X-ray contours overlaid on an optical image.

Because of the depth of the observation, sources were detected down to a luminosity of 2–5×10^{37} erg s^{-1}. This resulted in a de-
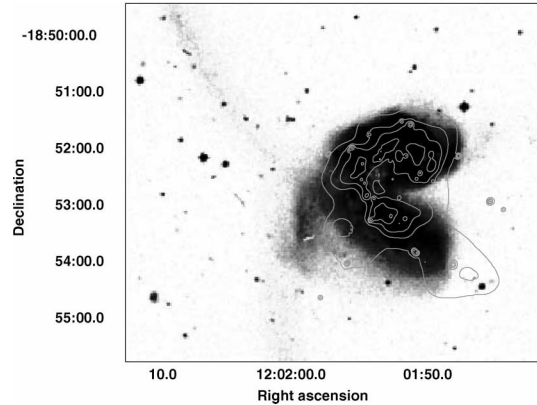

Figure 3. The Antennae, contours of adaptively smoothed 0.3–6.0 keV X-ray data from *Chandra* ACIS-S overlaid on an optical image from the UK Schmidt telescope.

tection of 120-point sources, 12 of these have been confirmed as ULXs. The integrated observation comprises seven separate pointings, enabling the variability of the point sources to be investigated.

Out of the 12 ULXs, four emit below 1×10^{39} erg s^{-1}, the lower luminosity threshold for a source to be classified as a ULX, in at least one observation. Further, one of the sources was observed in only one pointing, indicating that it is likely to be a transient, providing further evidence that ULXs are a heterogeneous class, comprising contributions from X-ray binary (XRB) systems, transient sources and also, possibly, intermediate-mass black holes (IMBHs).

The quality of the data has also lead to detailed mapping of the diffuse gas, investigating both the temperature and metallicity variation of the interstellar medium (ISM). 21 separate regions of the diffuse gas have been analysed, spectral fitting of these regions reveal that there is a variation in temperature of the diffuse gas from 0.2 to 0.9 keV and metallicities vary from regions of subsolar abundances to areas of emission displaying supersolar abundances, notably in both the nuclear regions and two hotspots in the northern loop of the disc (R1 and R2 reported in Fabbiano et al. 2003).

The morphology of the gas reveals that there are large-scale diffuse features; two large faint X-ray loops extending to the south of the system and a low surface brightness halo in the region surrounding the stellar discs extending out to ∼18 kpc from the nucleus of NGC 4039. The two loops have temperatures ranging from 0.29 to 0.34 keV and the low surface brightness halo has a nominal temperature of 0.23 keV. This cooler larger scale emission may be the aftermath of a superwind, possibly from the first encounter of the two systems, which took place ∼2–5 × 10^8 yr ago. The star formation rates (SFRs) within the two nuclei are 2.1 and 1.7 M$_\odot$ yr^{-1} and in the region where the discs overlap has been found to be 5.0 M$_\odot$ yr^{-1} (Mihos, Bothun & Richstone 1993).

2.4 Mrk 266

The next system within this sample, Mrk 266 (also NGC 5256), is a double nucleus system with a large gaseous envelope. Here, a summary of the galaxy properties are presented, with the full analysis and results of a recent *Chandra* observation detailed in Section 3.1.

This system lies at a distance of 115 Mpc and has an X-ray luminosity of 7.32×10^{41} erg s^{-1}. The two nuclei, originating from the progenitors, are thought to comprise a low-ionization nuclear emission-line region (LINER) with a powerful starburst component, to the north of the system, and a Seyfert type 2 to the south
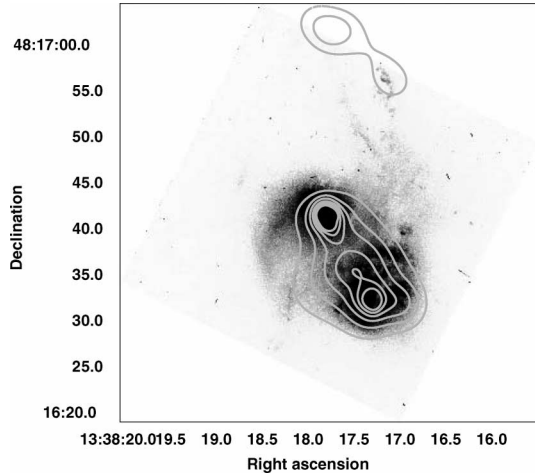
Figure 4. Mrk 266, contours of adaptively smoothed 0.3–8.0 keV X-ray data from *Chandra* ACIS-S overlaid on an optical image from WFPC2 on board the *HST*.

Figure 5. NGC 3256, contours of adaptively smoothed 0.3–8.0 keV X-ray data from *Chandra* ACIS-S overlaid on an optical image from WFPC2 on board the *HST*.

(Mazzarella et al. 1988). In addition to these sources, an area of enhanced emission has been detected between these nuclei, it is thought that this is caused by the collision of the two discs. Prior to a 20-ks *Chandra* observation of Mrk 266, made in 2001, this feature had not been seen in X-rays before. However, due to *Chandra's* superior spatial resolution, it is now possible to distinguish this feature. This can be seen in Fig. 4, where the adaptively smoothed, full band X-ray contours (0.3–8.0 keV) overlaid on an image from the Wide Field and Planetary Camera 2 (WFPC2), on board The *Hubble Space Telescope* (*HST*) are shown.

In addition to the central emission from the colliding galaxies, a large X-ray gas cloud can be seen to the north of the system. From a *ROSAT* observation it was proposed that this feature is a superwind, driven by the effect of the starburst's supernovae (SNe) and stellar winds from the centre of the system (Wang, Heckman & Weaver 1997). Kollatschny & Kowatsch (1998) argue that an X-ray 'jet', arising from a centrally powered superwind, is unlikely due to both the non-radial geometry of the emission and also the bright X-ray emission of the feature. They suggest that the most plausible mechanism to explain the 'jet' is from excitation by hot post-shock gas, although they do not conclude where the energy to power this feature would arise from. From the *Chandra* observation we speculate that the northern emission observed could also arise from star formation taking place in a tidal arm that has been stripped from the galaxy during an earlier interaction. The exact nature of this emission is discussed in detail in Section 3.1.4.

2.5 NGC 3256

The most X-ray luminous system in our sample, NGC 3256, is a powerful ultraluminous infrared galaxy (ULIRG), lying at a distance of 56 Mpc. This merger system, like Mrk 266, has one common gaseous envelope containing the nuclei from its two parent galaxies. Lira et al. (2002) report on a 28-ks *Chandra* observation made in 2000. Contours of adaptively smoothed 0.2–8.0 keV X-ray emission overlaid on an optical image of the system are shown in Fig. 5.

The total X-ray luminosity of NGC 3256 is 7.87×10^{41} erg s^{-1} with ~70 per cent of the X-ray luminosity arising from the diffuse emission. 14 discrete X-ray sources were detected in this system, all of which have been classified as ULXs. Because of the high source detection threshold of this observation ($L_X = 1.4 \times$
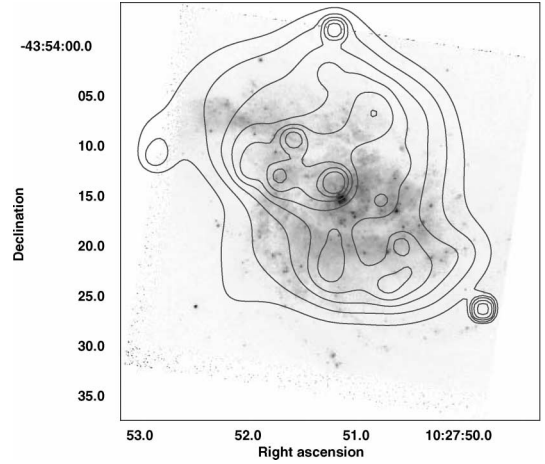
10^{39} erg s^{-1}) fainter point sources were not detected. Both galaxy nuclei are clearly detected in X-rays. The northern nucleus is a site of intense star formation, and UV spectra (Lípari et al. 2000) show strong absorption lines, implying the presence of massive young stars. The southern nucleus is heavily obscured and appears to be less active then the northern nucleus. It has been suggested that it hosts an active galactic nucleus (AGN), although there is no clear evidence of this provided in the X-ray data. The soft diffuse emission of the system can be described by two thermal components with a harder tail. The thermal plasma components exhibit temperatures of 0.6 and 0.9 keV and the hard component is thought to arise from a contribution from the lower luminosity X-ray point source population.

A kinematic study of the system (English et al. 2003) suggests that NGC 3256 is currently experiencing the starburst that just precedes the final core collision and, given the close proximity of the two nuclei, it is likely that this system has undergone more than one perigalactic approach. Assuming that the two tidal tails formed during the last closest encounter, the time that has elapsed since then can be estimated. This characteristic time-scale was calculated to be 500 Myr and it is thought that coalescence will take place in ~200 Myr.

2.6 Arp 220

The double nuclear system, Arp 220 (IC 4553/4554, UGC 09913), is a prototypical ULIRG, lying at a distance of 76 Mpc. The two nuclei have a separation of less than 0.5 kpc and are just at the point of coalescence. This complicated, dusty system has the highest value of L_{FIR} in our sample, which arises from the large reservoir of hot gas within the system. The mechanism by which this gas is heated is still currently under debate. Both the presence of a heavily shrouded AGN and intense nuclear starbursts have been suggested, along with a combination of both these energy sources contributing to the heating mechanism. A 60-ks *Chandra* observation of the system was made in 2000, and from these data both the nuclear and the extended emission have been analysed (Clements et al. 2002; McDowell et al. 2003). Fig. 6 shows the 0.2–1.0 keV adaptively smoothed X-ray emission, overlaid on an optical image.

The system hosts four ULXs, including the nuclei, no other point sources are detected. Three distinct regimes of large diffuse gas
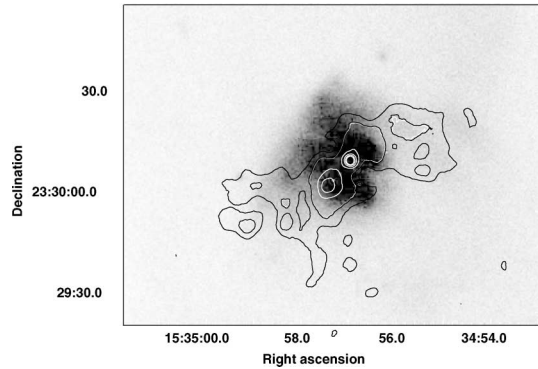
Figure 6. Arp 220, contours of adaptively smoothed 0.2–1.0 keV X-ray data from *Chandra* ACIS-S overlaid on an optical image from the Palomar 5-m telescope.
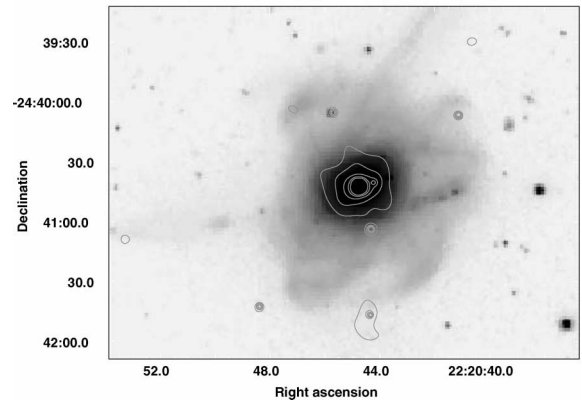

Figure 7. NGC 7252, contours of adaptively smoothed 0.3–7.0 keV X-ray data from *Chandra* ACIS-S overlaid on an optical image from the Las Campanas Observatory (LCO) 2.5-m telescope.

structures are observed; the circumnuclear region, a plume region and, further out, diffuse lobe regions. The circumnuclear region has both compact, hard nuclear emission that resides in the 1 kpc at the centre of the system and softer, more extended emission. It has been suggested that the hard component of this region arises from a significant point source population, emitting at a luminosity lower than $\sim 5 \times 10^{39}$ erg s^{-1}, the sensitivity threshold for this observation. Although, this could also be an AGN, albeit one emitting at a low luminosity.

The plume regions extend to the north-west and south-east of the system with a projected tip to tip length of ~ 10 kpc, these features are clearly seen in Fig. 6. The spectrum of the plumes include both hot (1–5 keV) and cooler (0.25 keV) thermal contributions. It is likely that these regions are associated with a superwind extending from the nuclear region as a consequence of the vigorous star formation that is taking place at the centre of the system. Beyond the plumes, two large, low surface brightness lobe regions have been observed extending from 10 to 15 kpc on either side of the nuclear region. These regions have been found to be cooler than the plumes (0.2–1.0 keV), although, due to the low number of counts, higher temperature gas residing in these regions cannot be ruled out.

It was noted by Heckman et al. (1996) that the plumes and lobes are 'misaligned' by $25°$–$30°$, they suggest that this could be due to a change in orientation of the system as the encounter has progressed. McDowell et al. (2003) propose that this misalignment is actually a consequence of the lobes being produced not by the superwinds in the system, but are a product of the merger itself. Tentative evidence to support this scenario is presented in an *INTEGRAL* observation by Colina, Arribas & Clements (2004).

2.7 NGC 7252

NGC 7252, the first example of a merger-remnant galaxy in our sample, is a prototypical merger galaxy at a distance of 63 Mpc. The central part of the system, a single relaxed body, displays an $r^{1/4}$ optical surface brightness profile typical of elliptical galaxies (Schweizer 1982). In addition to this relaxed nucleus, the galaxy exhibits complex loops and ripples, notably two long tidal tails, indicative of the merger history of this system. From both *UBVI* images taken with the WCFPT instrument on the *HST* (Miller et al. 1997) and *N*-body simulations (Hibbard & Mihos 1995), it has been estimated that nuclear coalescence took place ~ 1 Gyr ago.

A 28-ks *Chandra* observation, along with an *XMM–Newton* observation is reported in Nolan et al. (2004). Fig. 7 shows the 0.3–7.0 keV

adaptively smoothed *Chandra* X-ray contours overlaid on an optical image. A total of nine ULXs are detected within the optical confines of this system, a further five sources are also detected but at a lower significance ($<3\sigma$). The hot, diffuse gas of the system has been found to be fairly symmetrical and has an X-ray luminosity of 2.42×10^{40} erg s^{-1}. This is low when compared to luminosities from typical elliptical galaxies ($L_X \sim 10^{41-42}$ erg s^{-1}). The low luminosity of this system is possibly due to the young age of the galaxy and, over much longer time-scales, X-ray halo regeneration may increase the mass and hence luminosity of the gas within this system to levels seen in typical elliptical galaxies. From spectral modelling of the *XMM–Newton* data the X-ray emission from the nuclear region is found to emit at 0.72 and 0.36 keV. There is also a harder contribution that can be fitted with a power law, and it is expected that this is due to a lower luminosity point source population.

During the nuclear coalescence of NGC 7252 the SFR at the centre of the galaxy would have been massively enhanced. Now, as the reserve of gas becomes depleted, the SFR has fallen to one third of the value it would have been at its peak (Mihos et al. 1993), although its L_{FIR} is still enhanced when compared to normal quiescent galaxies.

2.8 Arp 222

Arp 222, or NGC 7727, is a post-merger galaxy at a slightly more advanced stage of evolution than NGC 7252 (Georgakakis, Forbes & Norris 2000). A CO observation (Crabtree & Smecker-Hane 1994) indicates that these systems are very similar in morphology and both host young cluster populations, however, Arp 222 seems to have a much smaller molecular gas content than NGC 7252. From a *K*-band observation (Rothberg & Joseph 2004) it has been found that the optical surface brightness profile of Arp 222 follows the de Vaucouleurs $r^{1/4}$ law, indicating that violent relaxation has taken place since the merger. From analysing the discrete structure of the galaxy, plumes extending from the nucleus were identified, these features indicate that the system has still not fully relaxed into a mature elliptical galaxy.

A 19-ks *Chandra* observation of the post-merger-remnant was carried out in 2001, and analysis and results from this observation are given in Section 3.2. Fig. 8 shows the 0.3–8.0 keV adaptively smoothed X-ray emission overlaid on an optical image. From this observation 15 point sources were detected, two of which are classified as ULXs. The X-ray luminosity of the diffuse gas in this system
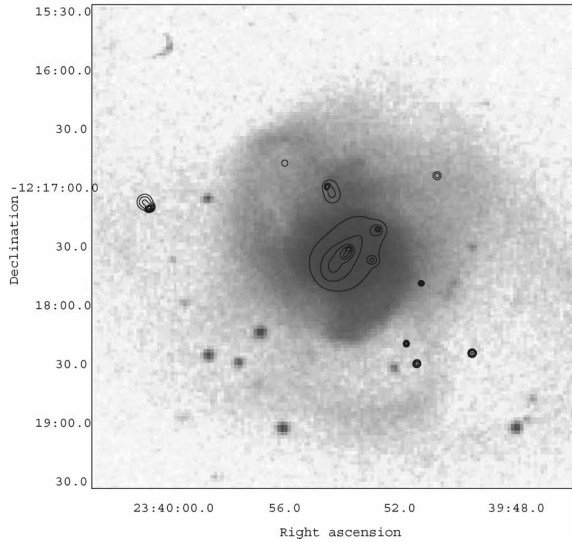
Figure 8. Arp 222, contours of adaptively smoothed 0.3–8.0 keV X-ray data from *Chandra* ACIS-S overlaid on an optical image from the UK Schmidt telescope.

Figure 9. NGC 1700, contours of adaptively smoothed 0.3–0.8 keV X-ray data from *Chandra* ACIS-S overlaid on an optical image from the UK Schmidt telescope.

is 6.52×10^{39} erg s^{-1}, much lower than the X-ray luminosity emitted from NGC 7252. This is likely to be due to the smaller gas content of Arp 222, which, as can be seen in Fig. 8, does not extend to the optical confines of the galaxy. From spectral modelling the global temperature of the diffuse gas in this system has been found to be 0.60 keV. The L_{FIR} value of the system is much lower than that of the previous systems and is similar to values seen in elliptical galaxies.

2.9 NGC 1700

The final system in our sample, NGC 1700, is a protoelliptical galaxy with a best age estimate of ∼3 Gyr (Brown et al. 2000). This galaxy possesses a kinematically distinct core and boxy isophotes at larger radii, it also contains two symmetrical tidal tails, a good indicator that this system formed through the merger of two, comparable mass, spiral galaxies. It has been suggested that it is the presence of these tidal features that causes the 'boxiness' of the galaxy (Brown et al. 2000). A 42-ks *Chandra* observation was made of the system in 2000, and the results of this are reported in Statler & McNamara (2002). Fig. 9 shows the 0.3–0.8 keV adaptively smoothed X-ray emission overlaid on an optical image of NGC 1700.

From this observation, 36 point sources are detected, six of which are classified as ULXs (Diehl & Statler, in preparation). The diffuse X-ray gas is well modelled by a single temperature thermal plasma at a temperature of 0.43 keV and has an X-ray luminosity of 1.47×10^{41} erg s^{-1}, similar to that of a mature elliptical galaxies. The change in morphology of the diffuse X-ray gas from the central elliptical region to the outer boxy region can clearly be seen in Fig. 9. Statler & McNamara (2002) suggest that the flattening of the isophotes is a consequence of an elliptical–spiral interaction, not a spiral–spiral merger as suggested by Brown et al. (2000). They argue that an interaction involving a pre-existing elliptical with a hot ISM, would lead to the channelling of the already hot gas into the systems common potential well. This gas, at sufficiently low densities, would then settle into a rotationally flattened cooling disc, as is observed. Currently, neither these two scenarios nor the suggestion
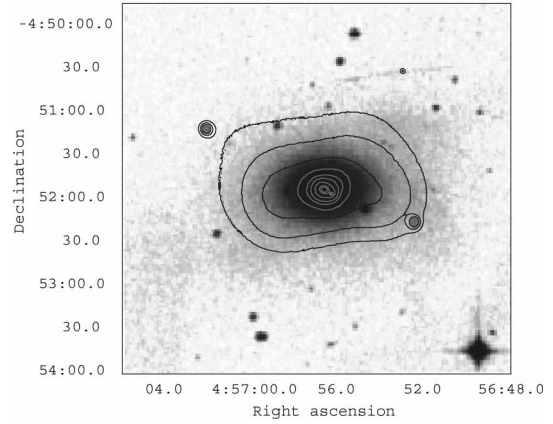
that the system could have formed from a three-body interaction (Statler, Smecker-Hane & Cecil 1996) can be ruled out.

3 *CHANDRA* OBSERVATIONS AND DATA ANALYSIS OF Mkn 266 AND Arp 222

Observations of Mrk 266 and Arp 222 were carried out with the Advanced CCD Imaging Spectrometer (ACIS-S) camera on board the *Chandra* X-ray Observatory. Mrk 266 was observed on 2001 November 2 with a total observation time of 19.7 ks and Arp 222 was observed on 2001 December 18 with a total observation time of 19.0 ks. The initial data processing to correct for the motion of the spacecraft and apply instrument calibration was carried out with the standard data processing (SDP) at the *Chandra* X-ray Center (CXC). The data products were then analysed using the CXC CIAO software suite (v3.2)[1] and HEASOFT (v5.3.1). The data were reprocessed, screened for bad pixels and time filtered to remove periods of high background (when counts deviated by more than 5σ above the mean). This resulted in a corrected exposure time of 18.5 ks for Mrk 266 and 18.8 ks for Arp 222. The full data analysis and results from these two observations are detailed in the following subsections.

3.1 Mrk 266

3.1.1 Overall X-ray structure

A 0.3–8.0 keV (from here on referred to as 'full band') *Chandra* image was created from the cleaned events file and adaptively smoothed using the CIAO task CSMOOTH which uses a smoothing kernel to preserve an approximately constant signal-to-noise ratio across the image, which was constrained to be between 2.6 and 4. In Fig. 10 both the optical image from the *HST* with the full band X-ray contours overlaid (left) and the 'true colour' image of the galaxy system (right) are shown. The 'true colour' image was created by combining three separate smoothed images in three energy bands: 0.3–0.8, 0.8–2.0 and 2.0–8.0 keV, using the same smoothing scale for each image. These energy bands correspond to red, green and blue, respectively. From these images it can be seen that the system is composed of two separate regions of X-ray emission. To the
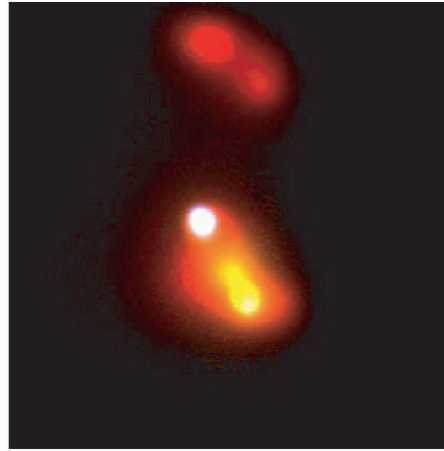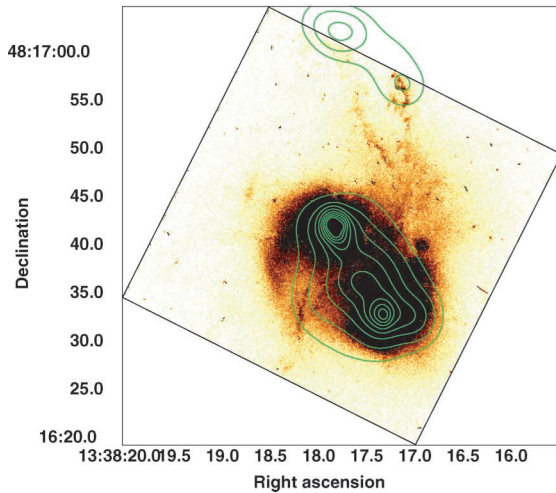
---

[1] http://asc.harvard.edu/ciao

Figure 10. Left: contours of adaptively smoothed 0.3–8.0 keV X-ray data from *Chandra* ACIS-S overlaid on an optical image from WFPC2 on board the *HST*. The black box indicates the plate boundary of the *HST* image. Right: shows the 'true colour' image of Mrk 266. Red corresponds to 0.3–0.8 keV, green to 0.8–2.0 keV and blue to 2.0–8.0 keV.

south of the images the central emission from the interacting galaxies can be seen. This comprises the two nuclei from the progenitor galaxies, a LINER to the north and a Seyfert 2 to the south, contained within a common gaseous envelope and a region of enhanced emission between the two nuclei. This region is coincident with a radio source reported in Mazzarella et al. (1988). It is likely that this enhanced emission is due to the interaction of the two galaxy discs. To the north of the images diffuse gas is detected and shows some correlation with emission seen in the *HST* image. The nature of this emission is discussed in detail in Section 3.1.4.

From the 'true colour' image it can be seen that the north-east nucleus emits in all three energy bands, whilst the south-west nuclear emission is not as hard. There is also some enhanced X-ray emission in the central region between the two nuclei. The X-ray emission surrounding these nuclei appears to be soft and diffuse with some suggestion of a superbubble to the south-east of the system.

3.1.2 Point source spatial and spectral analysis

Discrete X-ray sources were detected using the CIAO tool WAVDETECT. This was run on the full band image, over the 2, 4, 8, 16 pixel wavelet scales (where pixel width is 0.1 arcsec), with a significance threshold of 2.5×10^{-5}, which corresponds to one spurious source over a 200×200 pixel grid, the size of our image. Only four sources were detected in this range: the two nuclei and two regions in the diffuse northern feature. Both the regions in the northern emission contained less than 30 counts and had large detection regions of $r \geqslant 3.5$ arcsec and so were not defined as point sources. Instead, a spectrum was extracted from a region file containing all the northern emission. These two detections, along with the extraction and background extraction regions for the two nuclei, are shown in Fig. 11.

The two detected nuclear sources were extracted using the source region files created by WAVDETECT. The size of each region was selected to ensure that as many source photons as possible were detected whilst minimizing contamination from nearby sources and background. The background files were defined as a source free annulus surrounding and concentric with each source region file, to account for the variation of diffuse emission, and to minimize effects related to the spatial variation of the CCD response.
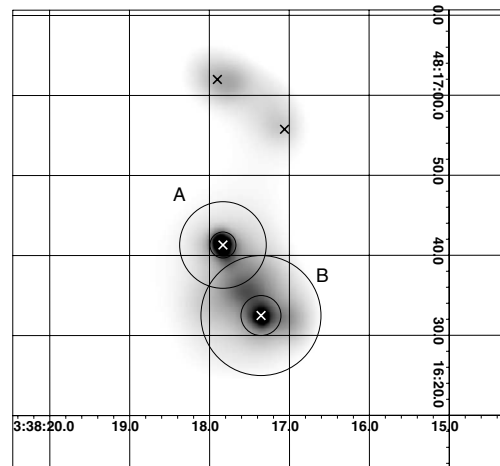

Figure 11. Adaptively smoothed 0.3–8.0 keV X-ray data from *Chandra* ACIS-S of Mrk 266, with WAVDETECT point source denoted with an 'X'. Extraction and background region files for sources A and B are also shown.

The source spectra for the two nuclei were created using the CIAO tool PSEXTRACT and fitted in XSPEC (v11.3.1). Because of the low number of counts in this observation the Cash statistic (Cash 1979) was used in preference to χ^2 when modelling the data. Both sources were well fitted with an absorbed thermal model plus an absorbed power law, the absorption component was fixed at the value out of our Galaxy (1.68×10^{20} atom cm^{-2}). The data were restricted to 0.3–6.0 keV, as energies below this have calibration uncertainties, and the spectra presented here do not have significant source flux above 6.0 keV. The parameters from these best-fitting models can be seen in Table 1; where columns 2 and 3 give the right ascension (RA) and declination (Dec.) (J2000), column 4 the count rate, column 5 the source significance, column 6 the Galactic value of N_H, column 7 kT, column 8 metallicity, column 9 power-law photon index (Γ) and columns 10 and 11 give the observed and intrinsic (i.e. corrected for absorption) luminosities.

From this table it can be seen that source A, the LINER, exhibits a remarkably flat power law of $0.02^{+0.25}_{-0.21}$. It is likely that part of the

Table 1. Sources detected in the 0.3–6.0 keV band within the Mrk 266 with a summary of point source spectral fits. Errors on the spectral fits parameters are given as 1σ for one interesting parameter from XSPEC. An F denotes that the value has been frozen.

Source	RA	Dec.	Count rate	Sig.	N_H	Spectral fit kT	Z	Γ	Luminosity (0.3–6.0 keV) $(10^{41}$ erg s$^{-1})$	
			$(\times 10^{-2}$ count s$^{-1})$	(σ)	$(\times 10^{20}$ atom cm$^{-2})$	(keV)	$(Z_\odot)$		Observed	Intrinsic
A	13:38:17.84	+48:16:41.2	1.90 ± 0.11	41.8	1.68 F	$0.80^{+0.07}_{-0.11}$	$0.59^{+1.50}_{-0.24}$	$0.02^{+0.25}_{-0.21}$	3.41 ± 0.17	3.47 ± 0.17
B	13:38:17.36	+48:16:32.5	0.90 ± 0.08	18.7	1.68 F	$0.88^{+0.08}_{-0.10}$	0.30 F	$1.13^{+0.49}_{-0.64}$	0.98 ± 0.07	1.04 ± 0.07

contribution to this component arises from unresolved point sources but the very flat slope of this fit suggests that some of the hard component is either heavily absorbed or dominated by reflection (Matt et al. 2000; Levenson et al. 2004). By including an absorber for the power-law component we can allow for this extra absorption, however, due to the low number of counts, when including this component the fit becomes unconstrained.

It is likely that the cause of this heavy obscuration is due to the strong starburst in this region. An observation by Sanders et al. (1986) found that Mrk 266 is rich in CO, indicating that this system contains a massive, warm reservoir of molecular gas to fuel this starburst, and the dynamic conditions that concentrate this material also serve to further obscure the LINER. The MEKAL component of the fit to this source arises from this starburst, which contributes 5.7×10^{40} erg s^{-1} to the total intrinsic luminosity of source A.

Source B, the southern nucleus, emits at a temperature of 0.88 keV and has a power-law slope of 1.13. This thermal component is likely to arise from the diffuse emission surrounding the nucleus, and the value of Γ is consistent with the interpretation of this nucleus being a Seyfert 2 (Cappi 2006). In previous X-ray surveys it has been found that up to ~75 per cent of Seyfert 2 objects are heavily obscured with $N_H \geqslant 10^{23}$ atom cm^{-2} (Risaliti, Maiolino & Salvati 1999). With the data we have from this observation the two-component model describes the spectrum well, and, due to the limited number of counts, a more complex model with an additional absorption component would overfit the data. In addition to this, Cappi (2006) have found from a recent survey of nearby Seyfert galaxies that these sources possess the entire range of N_H from 10^{20} to 10^{24} atom cm^{-2}, fairly continuously. Indicating that, although the southern nucleus could be heavily obscured, it is also possible that the two-component model described here is good indication of the properties of this source.

3.1.3 Diffuse emission spatial and spectral analysis

From the 'true colour' image of Mrk 266 it is clear that the galaxy contains significant amounts of diffuse gas, in both the northern feature and also surrounding the central galaxy. To investigate the nature of this diffuse emission, spectra were extracted from these two separate regions using the CIAO tool ACISSPEC, and fitted in XSPEC. Once again, due to the low number of counts, the Cash statistic was used when modelling the data.

The diffuse gas contained within the galaxy is not well described by a single temperature fit, and is better modelled with two temperature components. It is likely that the hotter gas contributing to this model arises from the enhanced emission seen between the two nuclei. To investigate this, the extraction region was divided into two separate parts: one, smaller region, to probe the impact area, where it is likely that the two discs have collided, and a second, larger region, covering the rest of the galaxy, but which excludes the inner impact region and the northern diffuse region. These, along with the
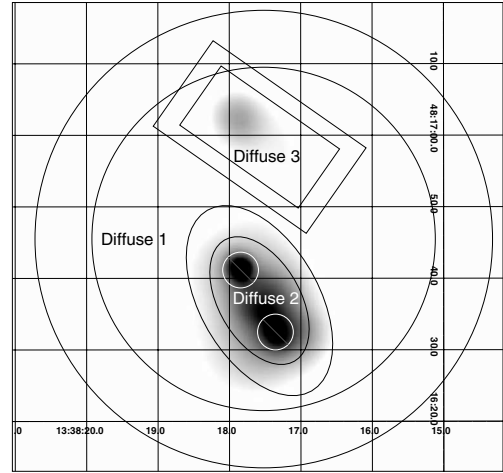
Figure 12. Adaptively smoothed 0.3–8.0 keV X-ray data from *Chandra* ACIS-S of Mrk 266, with extraction and background region for the diffuse gas shown. The background region files are selected to be source free annuli, surrounding and concentric with each extraction region file.

extraction region for the northern diffuse emission and the associated background regions, are shown in Fig. 12. The two separate regions, diffuse 1 and diffuse 2, are both well described with single component MEKAL fits, exhibiting the same temperatures that were fitted in the two temperature model. The northern region is also well described with a single component MEKAL fit. The parameters from the best-fitting models for these regions, along with their X-ray luminosities, are shown in Table 2.

From this table it can be seen that the diffuse gas within the galaxy system, diffuse 1, exhibits a temperature of 0.52 keV, a fairly typical temperature for gas in interacting galaxies (RP98). The impact region, diffuse 2, has a higher temperature of 1.07 keV. This is, within errors, the same temperature attained from the higher temperature contribution from the two component MEKAL fit of the combined spectrum for diffuse 1 and diffuse 2, indicating that the higher temperature from this fit was a consequence of the gas arising from this impact area.

The northern emission appears spectrally distinct from the surrounding diffuse gas and has been found to emit at a cooler temperature of 0.30 keV. With this *Chandra* data it has also been found that this region has a much lower luminosity than the one derived in Kollatschny & Kowatsch (1998), who report on a *ROSAT* High Resolution Imager (HRI) observation of the galaxy and find the X-ray luminosity of this region to be 3.1×10^{41} erg s^{-1}, as opposed to 6.9×10^{40} erg s^{-1}, as reported in this work. However, in Kollatschny & Kowatsch (1998) this X-ray luminosity is derived from assuming that the relative number of HRI counts is directly proportional to their share of the integrated X-ray flux, with the total luminosity of

Table 2. Summary of the spectral fits of the diffuse gas regions in Mrk 266. Errors on the spectral fits parameters are given as 1σ for one interesting parameter from XSPEC. An F denotes that the value has been frozen.

Diffuse region	N_H ($\times 10^{20}$ atom cm^{-2})	kT (keV)	Z ($Z_\odot$)	Luminosity (0.3–6.0 keV) (10^{40} erg s^{-1}) Observed	Intrinsic
Diffuse 1	1.68 F	$0.52^{+0.06}_{-0.06}$	$0.23^{+0.05}_{-0.03}$	9.88 ± 0.50	10.92 ± 0.50
Diffuse 2	1.68 F	$1.07^{+0.06}_{-0.09}$	$0.22^{+0.15}_{-0.08}$	8.10 ± 0.49	9.83 ± 0.53
Diffuse 3	1.68 F	$0.30^{+0.02}_{-0.03}$	0.30 F	6.10 ± 0.49	6.90 ± 0.55

the system being derived from the *ROSAT* Position Sensitive Proportional Counter (PSPC) observation of the system and consequently has large uncertainties associated with it.

3.1.4 Nature of the northern emission

The origin of the diffuse emission to the north of the system is still the subject of debate. There have been a number of suggestions as to how this feature has been formed. From HRI and PSPC observations with *ROSAT*, Wang et al. (1997) suggest that it is an outflow, driven by the mechanical energy of the SNe and stellar winds in the starburst. A subsequent paper (Kollatschny & Kowatsch 1998), investigating both the HRI observation and optical *B*, *V*, *R* images of Mrk 266, argued that the scenario proposed by Wang et al. (1997) is unlikely, due to both the high luminosity of the 'jet' and also its non-radial geometry. They instead suggest that the mechanism that gives rise to the 'jet' is excitation by hot post-shock gas, although they do not conclude where the energy to power this feature would arise from.

A tridimensional spectrophotometric study by Ishigaki et al. (2000) investigated the Hα, [O III] and [S II] emission lines within Mrk 266. Fig. 13 shows the Hα contours from this observation, overlaid on the full band, adaptively smoothed, *Chandra* X-ray emission. As can be seen, the enhanced regions of Hα in the northern region are coincident with the two X-ray regions detected with WAVDETECT (see Fig. 11). Some caution should be exercised when interpreting this plot due to the uncertainty in the astrometry, which we conservatively estimate to be 2 arcsec (1.1 kpc). Even so, the correlation
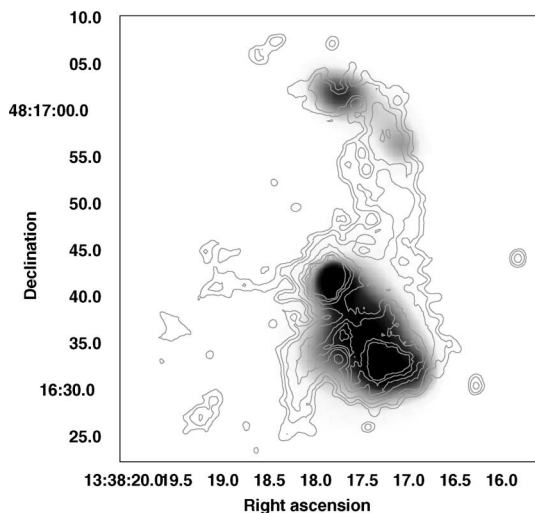

Figure 13. Adaptively smoothed 0.3–8.0 keV X-ray data from *Chandra* ACIS-S of Mrk 266. Hα contours from Ishigaki et al. (2000) are overlaid.

between the X-ray and Hα is striking, suggesting that this region to the north of the system is a site of star formation, possibly a tidal arm that has been stripped from the southern progenitor during the merger process. This interpretation is strengthened by the fact that both the *HST* (Fig. 10) and Hα emission seem to connect with the dust lanes around the southern nucleus (Ishigaki et al. 2000).

As shown in the previous section, the luminosity arising from the diffuse gas within the northern feature is 6.9×10^{40} erg s^{-1}. Given that our spectral fit to the data indicates that this emission arises from a thermal component, and both the *HST* and Hα emission indicate that there is star formation within this region, the origin of these X-rays could come from SNe. Making some assumptions about the geometry of the emitting region of this northern feature the thermal energy of the gas can be derived. First, the volume, V, of the diffuse northern emission has been assumed to be an ellipsoid, with symmetry about the longer axis. The fitted emission measure is equal to $\eta n_e^2 V$ and can be used to infer the mean particle number density n_e, with the filling factor, η, assumed to be 1. This factor represents the fraction of volume filled by the emitting gas. Although we have assumed this to be 1 in our calculations, there is evidence from hydrodynamical simulations to suggest this value could be $\leqslant 2$ per cent (Strickland & Stevens 2000). The mean electron density is then used to derive the total gas mass M_{gas}, which then leads to the thermal energy E_{th} of the hot gas. From these assumptions E_{th} has been calculated to be between 6.72×10^{54} erg (for $\eta = 0.02$) and 3.36×10^{56} erg (for $\eta = 1$).

By deriving the SN rate, r_{SN}, for this region, the energy arising from SNe can be calculated. Davies, Ward & Sugai (2000) calculate r_{SN} for the LINER in Mrk 266, using the relation derived in Condon & Yin (1990),

$$L_{NT}[\text{WHz}^{-1}] \sim 1.3 \times 10^{23} (\upsilon[\text{GHz}])^{-0.8} r_{SN}[\text{yr}^{-1}], \qquad (1)$$

and the 20-cm radio continuum (Mazzarella et al. 1988). Where L_{NT} is the calculated power and υ is the frequency of the observation. From this they calculate r_{SN} to be 0.45 SN yr^{-1}.

For the northern diffuse emission, Mazzarella et al. (1988) find a power of 8.9×10^{21} WHz^{-1}, using this value and the above equation we find $r_{SN} = 0.05$ SN yr^{-1} for this region. From Mattila & Meikle (2001) it has been found that it is more appropriate to use L_{FIR} to calculate r_{SN} in starburst galaxies but, as we only have L_{FIR} for the whole system, we would greatly overestimate the SN rate, and consequently, we will use the rate of 0.05 SN yr^{-1} we have derived from the 20-cm continuum data.

From Davies et al. (2000), models of the star formation time-scales have been derived for the LINER. Furthermore, although these models give a fairly poorly constrained age (20–500 Myr), by making the assumption that this is a proxy for the time-scales of star formation taking place in the northern diffuse emission, the number of SNe formed in this time can be estimated. Given that we

also make the assumption that a massive star takes $\sim 1 \times 10^7$ yr to evolve into a SN, we calculate the number of SNe formed in this time to be 5×10^5–2.5×10^7. If each SN releases $\sim 1 \times 10^{51}$ erg, the total thermal energy available will be between $\sim 5 \times 10^{56}$ and $\sim 2.5 \times 10^{58}$ erg, thus demonstrating that the observed luminosity in the northern diffuse emission could arise from the contribution of star formation alone.

The reason that both Wang et al. (1997) and Kollatschny & Kowatsch (1998) prefer an outflow scenario to that of tidal stripping to explain this northern feature is due to the presence of optical emission in a highly excited state within this feature. These line ratios, coupled with the electron temperature calculated for this region, cannot be explained by thermal collisional ionization, and are likely to arise through either photoionization or shock excitation. Wang et al. (1997) and Kollatschny & Kowatsch (1998) both suggest that these shocks arise from a 'jet', outflowing from the central galaxy. However, Ishigaki et al. (2000) propose that the northern emission is photoionized by radiation from the Seyfert nucleus and, therefore, excitation by shocks is not required to explain the high excitation emission lines that are observed.

The present study adds further evidence to this debate. With the higher resolution provided by *Chandra*, the structure of the northern emission can now be resolved. From this it can be seen that the northern feature is curved, and the X-ray emission appears to be 'clumpy', with the two most intense areas of X-ray emission coincident with the Hα emission (see Fig. 13). These are not features which indicate a superwind. Furthermore, the morphology of this region traces that of the optical emission, which is highly suggestive that these two features are connected. Consequently, we propose that the most likely source of this X-ray emission is star formation taking place within a tidal arm that has been stripped out from one of the progenitors during the merger of the two galaxies.

3.1.5 The south-east extension

To the south-east of the central galaxy region there is some suggestion of X-ray extension, which appears to be coincident with filaments seen in the *HST* image, just beginning to break out of the galactic disc (Fig. 10). Given the low count statistics in this observation we cannot extract spectra for this region alone. However, from the morphology of the X-ray emission, coupled with the Hα

emission, there is some indication that this region is a site of star formation just on the point of break-out from the gaseous envelope of the central system. This scenario is preferred to the one suggested in the case of the northern emission as there is additional evidence of an outflow feature from the starburst region around the LINER (Ishigaki et al. 2000). This outflow could be beginning to sweep the dust out of the galaxy, indicating that this system is in the stage just prior to the outbreak of large-scale galactic winds throughout the system. Of course, alternatively, this feature could be a small-scale version of the northern emission, particularly given its coincidence with optical emission seen with the *HST*. However, without spectral information to investigate the nature of this object, neither scenario can be ruled out.

3.2 Arp 222

3.2.1 Overall X-ray structure

A full band adaptively smoothed *Chandra* image of Arp 222 was produced using the same tools and techniques as described in Section 3.1.1. In Fig. 14 both the optical image from the UK Schmidt telescope, with the smoothed full band X-ray contours overlaid (left), and the 'true colour' image (right) of Arp 222 are shown. The true colour image was produced using the same methods as described in Section 3.1.1.

From these images it can be seen that there is some diffuse gas at the centre of the galaxy, but this emission does not extend out to the optical confines of the system. In addition to the diffuse gas, a number of point sources are found through out the galaxy. From the 'true colour' image, the white appearance of the nucleus indicates that it emits in all three energy bands, whilst the other point sources can be seen to be softer.

3.2.2 Spatial and spectral analysis

X-ray point sources were searched for using the CIAO tool WAVDETECT. This was run on the full band image, over the 2, 4, 8, 16 pixel wavelet scales (where pixel width is 0.5 arcsec), with a significance threshold of 2.8×10^{-6}, which corresponds to one spurious source over a 600×600 pixel grid, the size of our image. 24 sources were detected in this full band range, these were then limited to
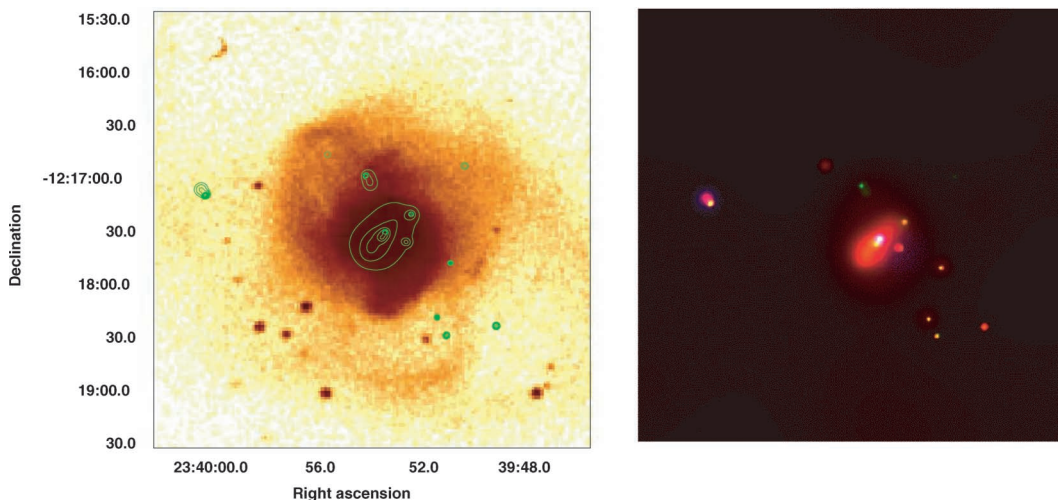

Figure 14. Left: contours of adaptively smoothed 0.3–8.0 keV X-ray data from *Chandra* ACIS-S overlaid on an optical image from the UK Schmidt telescope. Right: shows the 'true colour' image of Arp 222. Red corresponds to 0.3–0.8 keV, green to 0.8–2.0 keV and blue to 2.0–8.0 keV.
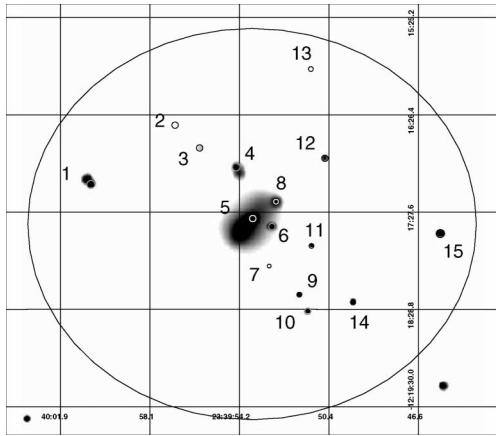
Figure 15. Adaptively smoothed 0.3–8.0 keV X-ray data from *Chandra* ACIS-S of Arp 222, with point sources detected by WAVDETECT indicated. The D_{25} ellipse is also shown.

those that lie within the D_{25} ellipse of the galaxy, reducing the number to 15 detected sources. These regions, along with the D_{25} ellipse are shown in Fig. 15. From using the *Chandra Deep Field*-South number counts (Giacconi et al. 2001) we estimate two to three of these sources to be background objects.

Spectra for the point sources were extracted using the CIAO tool PSEXTRACT with region and background region files selected in the same way as described in Section 3.1.3. Of the 15 detected sources, only one, source 5, emitted sufficient counts to be modelled individually, the other 14 sources were fitted simultaneously. The spectrum of the diffuse gas was extracted with the CIAO tool ACISSPEC, from a region file centred on source 5, with a radius of 45 arcsec. The background region file was defined to be a source free annulus surrounding and concentric with the region file. Once again, due to the low number of counts, the Cash statistic was used in preference to χ^2. Both the combined sources and source 5 were well described by single component, power-law models. Furthermore, from this combined fit model, the luminosities for each individual source were derived. The diffuse gas was well fitted by a single

component MEKAL model. These spectral fits are summarized in Table 3, where column 1 gives the source identification number, columns 2 and 3 give the RA and Dec. (J2000), column 4 the Galactic value of $N_{\rm H}$, column 5 kT, column 6 metallicity, column 7 Γ and columns 8 and 9 give the observed and intrinsic luminosities.

From this table it can be seen that the best-fitting spectral index for the combined sources is $\Gamma = 1.72$, a typical value for XRBs in, what can be described as, a low/hard state (Soria & Wu 2003). For the central source, source 5, the best-fitting model has shown that the spectral state is much softer, with $\Gamma = 2.15$. This value is consistent with it also being an XRB, but this time in a high/soft state (Colbert et al. 2004). This source, along with source 1, has been found to be a ULX. Given the quiescent nature of the galaxy, and that the time since the last episode of widespread star formation has been shown to be ∼1.2 Gyr ago (Georgakakis et al. 2000), this indicates that these sources are likely to arise from low-mass X-ray binaries (LMXRBs), not high-mass X-ray binaries (HMXRBs) as has been seen in younger merger systems within this sample.

The amount of diffuse gas within the system is smaller than in mature elliptical galaxies, and, as mentioned previously, does not extend out to the optical confines of the system. The temperature of the gas, 0.6 keV, has been found to be comparable to that of other interacting systems, but the diffuse gas exhibits a lower X-ray luminosity (6.52×10^{39} erg s^{-1}) than the other systems within this sample. The low gas content of Arp 222 is further seen from CO observations of the galaxy (Crabtree & Smecker-Hane 1994). From this *Chandra* observation it can be seen that this system is X-ray faint and does not currently resemble a mature elliptical galaxy, although may at a greater dynamical age.

4 THE EVOLUTION OF MERGING GALAXIES

4.1 Multiwavelength evolution sequence

To gain a greater understanding of the merger process of galaxy pairs, in addition to the X-ray luminosity of each system, *B* band, *K* band and FIR luminosities have been obtained to study how each of these luminosity diagnostics evolve along the chronological

Table 3. A summary of the best-fitting parameters for the diffuse gas and point sources detected in the 0.3–6.0 keV band within Arp 222. Errors on the spectral fits parameters are given as 1σ for one interesting parameter from XSPEC. An F denotes that the value has been frozen.

Source	RA	Dec.	$N_{\rm H}$ ($\times 10^{20}$ atom cm^{-2})	Spectral fit kT (keV)	Z ($Z_\odot$)	Γ	Luminosity (0.3–6.0 keV) (10^{39} erg s^{-1}) Observed	Intrinsic
1	23:40:00.61	−12:17:10.2	2.75 F	–	–	1.72 F	0.99 ± 0.17	1.07 ± 0.17
2	23:39:57.01	−12:16:33.0	2.75 F	–	–	1.72 F	0.31 ± 0.16	0.32 ± 0.16
3	23:39:55.95	−12:16:47.3	2.75 F	–	–	1.72 F	0.19 ± 0.07	0.21 ± 0.08
4	23:39:54.37	−12:16:59.1	2.75 F	–	–	1.72 F	0.45 ± 0.11	0.48 ± 0.12
5	23:39:53.67	−12:17:31.6	2.75 F	–	–	$2.15^{+0.37}_{-0.36}$	1.74 ± 0.21	1.97 ± 0.24
6	23:39:52.84	−12:17:36.8	2.75 F	–	–	1.72 F	0.37 ± 0.11	0.40 ± 0.12
7	23:39:52.97	−12:18:01.5	2.75 F	–	–	1.72 F	0.20 ± 0.09	0.21 ± 0.09
8	23:39:52.67	−12:17:21.1	2.75 F	–	–	1.72 F	0.43 ± 0.11	0.46 ± 0.12
9	23:39:51.67	−12:18:19.6	2.75 F	–	–	1.72 F	0.52 ± 0.14	0.54 ± 0.15
10	23:39:51.31	−12:18:30.0	2.75 F	–	–	1.72 F	0.35 ± 0.11	0.37 ± 0.11
11	23:39:51.15	−12:17:48.8	2.75 F	–	–	1.72 F	0.38 ± 0.11	0.42 ± 0.13
12	23:39:50.57	−12:16:53.7	2.75 F	–	–	1.72 F	0.28 ± 0.09	0.30 ± 0.10
13	23:39:51.18	−12:15:57.6	2.75 F	–	–	1.72 F	0.30 ± 0.12	0.31 ± 0.13
14	23:39:49.36	−12:18:24.4	2.75 F	–	–	1.72 F	0.38 ± 0.11	0.40 ± 0.12
15	23:39:45.63	−12:17:41.2	2.75 F	–	–	1.72 F	0.21 ± 0.12	0.55 ± 0.13
Diffuse	23:39:53.67	−12:17:31.6	2.75 F	$0.60^{+0.07}_{-0.06}$	$0.08^{+0.06}_{-0.02}$	–	5.48 ± 0.28	6.52 ± 0.33

Table 4. The fundamental properties of all the systems within this sample. Columns are explained in the text.

Galaxy system	Distance (Mpc)	Merger age (Myr)	L_X (0.3–6.0 keV) ($\times 10^{40}$ erg s^{-1})	L_{diff}	Log L_{FIR} (erg s^{-1})	Log L_B (erg s^{-1})	Log L_K (erg s^{-1})
Arp 270	28	−650	2.95	28	43.63	43.72	43.37
The Mice	88	−500	6.01	31	44.12	44.07	44.04
The Antennae	19	−400	6.97	54	43.95	43.98	44.64
Mrk 266	115	−300	73.18	41	44.75	44.30	44.38
NGC 3256	56	−200	87.70	80	45.19	44.42	45.22
Arp 220	76	0	23.70	44	45.50	43.97	44.78
NGC 7252	63	1000	6.17	31	44.00	44.40	44.61
Arp 222	23	1200	1.46	45	$\geqslant$42.37	43.92	44.84
NGC 1700	54	3000	17.58	83	42.91	44.32	45.15

sequence. In the case of systems where the X-ray luminosity has been obtained from the literature, the stated band has been converted into the 0.3–6.0 band used in this paper by assuming canonical models of the two X-ray components. For the diffuse gas, a MEKAL model with a gas temperature of 0.5 keV has been assumed, and for the point source population a power-law model with a photon index of 1.5 has been adopted.

These luminosities are given in Table 4, where column 1 gives the system name, column 2 the distance to the object, column 3 the merger age, with nuclear coalescence being defined as 0 Myr, column 4 the total (0.3–6.0 keV) intrinsic X-ray luminosity from the *Chandra* observation, column 5 the percentage of luminosity arising from the diffuse gas (per cent L_{diff}), column 6 L_{FIR}, column 7 L_B and column 8 gives L_K.

The FIR luminosities are calculated using the expression (Devereux & Eales 1989)

$$L_{FIR} = 3.65 \times 10^5 (2.58 S_{60\,\mu m} + S_{100\,\mu m}]D^2\, L_\odot, \tag{2}$$

with *IRAS* 60- and 100-μm fluxes taken from the *IRAS* Point Source Catalogue (Moshir 1990). The optical (*B*) luminosities were calculated as in Tully (1988):

$$\log L_B,\ (L_\odot) = 12.192 - 0.4 B_T + 2 \log D, \tag{3}$$

where B_T is the blue apparent magnitude and *D* is the distance in Mpc. Values of blue apparent magnitude were taken from de Vaucouleurs et al. (1991) (the value for The Mice was taken from NGC 2000.0 Dreyer 1988). The values of L_K are derived using the relation given in Seigar (2005):

$$\log L_K = 11.364 - 0.4 K_T + \log(1 + Z) + 2 \log D, \tag{4}$$

where K_T is the *K*-band apparent magnitude, *Z* is the galaxy redshift and *D* is the distance in Mpc. Apparent *K*-band magnitudes were taken from the 2MASS survey.

To calculate the value of per cent L_{diff} for each system, the contribution to the luminosity of the diffuse gas that arises from unresolved low luminosity point sources had to be estimated and removed. This was done in a number of ways: in the case of systems for which we have access to the reduced data (the Mice, Mrk 266 and Arp 222), an additional power-law component with a photon index of 1.5 was included in the spectral fit of the diffuse emission. It was then assumed that the luminosity of this component arises from unresolved point sources within the system. Additionally, for Mrk 266, it was assumed that the MEKAL component of the point source fits arises from the diffuse gas surrounding the LINER and Seyfert. In the cases of Arp 270 and NGC 7252, estimates of the contribution of

the unresolved point sources to the total diffuse luminosity has already been made in Brassington et al. (2005) and Nolan et al. (2004), respectively.

For the systems we have taken from the literature, the 'universal luminosity function' (ULF), derived by Grimm, Gilfanov & Sunyaev (2003), was used to predict the flux from unresolved low-luminosity sources. The predicted XRB luminosity function is

$$N(>L) = 5.4\, \text{SFR} \left(L_{38}^{-0.61} - 210^{-0.61} \right), \tag{5}$$

where $L_{38} = L/10^{38}$ erg s^{-1} and the factor 210 arises from the upper luminosity cut-off of 2.1×10^{40} erg s^{-1}. SFR was estimated from the population of brighter point sources detected above the completeness limit from the *Chandra* observations. In the case of The Antennae, point sources were detected down to a luminosity of 5×10^{37} erg s^{-1} and therefore no correction was required for this system.

As mentioned previously, one of the main difficulties in compiling an evolutionary sequence such as this is assigning an age to each of these systems. The way in which these estimates were made is described in Section 2, but another important point that was not discussed is that when constructing an evolutionary sample, the absolute time-scale of the merger process must be considered. From *N*-body simulations (Mihos & Hernquist 1996) it is clear that from the first initial strong interaction between equal-mass mergers, through to their nuclear coalescence, takes ~700 Myr. What is not so well defined is the amount of time that elapses between coalescence and the relaxation of the galaxy into a system resembling a mature elliptical galaxy. Within the sample presented here, this issue has been addressed by selecting a greater dynamical range than has previously been studied. By doing this it is hoped that the transition between young merger remnants to relaxed mature ellipticals can be observed, and therefore a more complete picture of the merger process can be obtained.

Although these merger systems are being compared to establish a single evolutionary sequence, it should be remembered that nine individual systems, not nine examples of one merger at different stages of its evolution, are being looked at. Consequently, although the trends that have been identified here should be a good indicator of how X-ray emission evolves during the merger process, due to the careful selection criteria outlined in Section 2, it is likely that other merger pair systems will exhibit different X-ray properties. These variations are likely to arise due to the unique interaction parameters associated with each merger system, as well as the variation of gas content and mass of individual galaxies within each system.

With the multiwavelength luminosities that have been collected for each system (Table 4), the evolution of the galaxy properties along the merger process has been investigated. The activity levels,
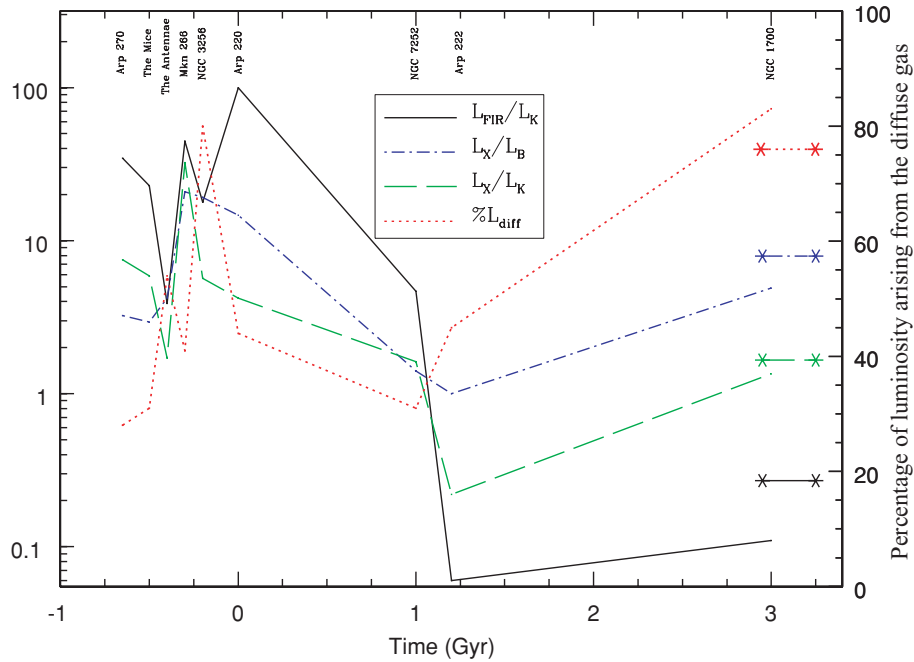
Figure 16. The evolution of X-ray luminosity in merging galaxies. Shown are L_{FIR}/L_K (solid line), L_X/L_B (dot–dash line), L_X/L_K (dashed line) and per cent L_{diff}, plotted as a function of merger age, where 0 age is defined to be the time of nuclear coalescence. All luminosity ratios (L_{FIR}/L_K, L_X/L_B and L_X/L_K) are normalized to the spiral galaxy NGC 2403. Per cent L_{diff} is plotted on a linear scale, shown on the right-hand y-axis of the plot and is an absolute value. Per cent L_{diff} for NGC 2403 is 12 per cent. The horizontal lines to the right of the plot indicate L_{FIR}/L_K, L_X/L_B, L_X/L_K and per cent L_{diff} for NGC 2434, a typical elliptical galaxy.

a proxy for star formation normalized by galaxy mass, are indicated by L_{FIR}/L_K. To investigate the variation of L_X, scaled by galaxy mass for each system, both the B-band and the K-band luminosities, L_X/L_B and L_X/L_K have been used. Both of these have been used as normalization values as L_B can become greatly enhanced during periods of star formation due to the presence of young stars, indicating that L_K is likely to provide a more reliable tracer of galaxy mass. Therefore, by plotting L_X against both of these values, how great this effect is can be observed.

These ratios are shown in Fig. 16, where not only the luminosity ratios but also the percentage of luminosity arising from diffuse gas (per cent L_{diff}) as a function of merger age have been plotted. L_{FIR}/L_K (solid line), L_X/L_B (dot–dash line) and L_X/L_K (dashed line) have been normalized to the typical spiral galaxy, NGC 2403. Whilst per cent L_{diff} (dotted line) is plotted on the right-hand y-axis of the plot, as an absolute value, where per cent L_{diff} for NGC 2403 is 12 per cent. The horizontal lines to the right of the plot indicate L_{FIR}/L_K, L_X/L_B, L_X/L_K and per cent L_{diff} for NGC 2434, a typical elliptical galaxy (Diehl & Statler, in preparation).

The system NGC 2403 was selected to represent a typical spiral galaxy. This system was chosen due to its close proximity ($D = 3.2$ Mpc), the fact that it does not have a high level of star-forming

activity and that it does not host an AGN (Schlegel & Pannuti 2003). NGC 2434 was selected to represent a typical elliptical galaxy. At a distance of 22 Mpc, this system is close enough to enable the point source population to be disentangled from the hot gas, allowing this diffuse emission to be modelled (Diehl & Statler, in preparation), this systems also exhibits the quiescent levels of star formation normally associated with such galaxies. Table 5 shows the properties for both of these systems, with columns as in Table 4.

Another factor that must be considered when plotting these luminosity ratios is the AGN that is hosted by Mrk 266. This is the only system within the sample that has a confirmed AGN, and as such, it is expected to be significantly more luminous than the other systems. Therefore, the values of L_X/L_B, L_X/L_K and per cent L_{diff} have been calculated for Mrk 266, both including and excluding the contribution from the Seyfert. As shown in Table 1, this nucleus is not a powerful AGN, instead it is close to the Seyfert–LINER borderline, and therefore, the total value of L_X only reduces by 14 per cent if it is excluded, with the value of per cent L_{diff} rising to 48 per cent. When the reduced luminosity is used to derive the luminosity ratios for Mrk 266, the change in Fig. 16 is very small, and the overall trends exhibited by these ratios are preserved.

Table 5. Properties of the typical spiral (NGC 2403) and the typical elliptical (NGC 2434) used in Fig. 16. Columns as in Table 4.

Galaxy system	Distance (Mpc)	L_X (0.3–6.0 keV) ($\times 10^{40}$ erg s^{-1})	L_{diff}	Log L_{FIR} (erg s^{-1})	Log L_B (erg s^{-1})	Log L_K (erg s^{-1})
NGC 2403	3	0.29	12	42.21	43.22	43.49
NGC 2434	22	4.82	76	41.96	43.54	44.49

4.2 Arp 220: the normalization of the universal luminosity function

Grimm et al. (2003) considered a number of SFR indicators for each galaxy within their sample. This was done, as there is considerable scatter in the SFR estimates obtained from different indicators. To calculate an 'adopted' SFR for each galaxy, indicators that deviated significantly from the other values were disregarded, and the remaining indicators were averaged to give a final value used in subsequent calculations.

In the present work, the SFR was estimated from the brighter point sources, detected from the *Chandra* observations. To further investigate the normalization of the ULF, SFR indicators, derived from L_{FIR}, using the expression (Rosa-González, Terlevich & Terlevich 2002)

$$SFR_{FIR} = 4.5 \times 10^{-44} L_{FIR} \, (\text{erg s}^{-1}) \qquad (6)$$

have also been used to estimate the luminosity arising from the unresolved point sources. This ULF correction, using the SFR indicator derived from L_{FIR}, has been calculated for the most active system within our sample, Arp 220. From this correction, a luminosity of $5.05 \times 10^{41} \, \text{erg s}^{-1}$ has been derived for the low luminosity ($L_X \leqslant 5 \times 10^{39} \, \text{erg s}^{-1}$) point sources. This value is almost two times greater than the *total* observed luminosity of Arp 220 (see Table 4), indicating that using L_{FIR} as a SFR in the ULF must greatly overestimate the point source population for this system. To ensure that the value calculated in equation (2) was consistent with other observations, additional L_{FIR} values were obtained (log L_{FIR} = 45.86, David, Jones & Forman 1992 and log L_{FIR} = 45.54, Liu & Kennicutt 1995). Averaging these values gives log L_{FIR} = 45.73 for Arp 220, similar to the value given in Table 4.

To investigate this further, we compare the observed population of brighter sources with that predicted using the ULF. From the *Chandra* observation, four sources with $L_X \geqslant 5 \times 10^{39} \, \text{erg s}^{-1}$ are detected in Arp 220. Using the SFR derived from L_{FIR} in equation (5), the bright point source population is estimated to be 10 times larger, with 41 discrete sources predicted. This demonstrates that, in the case of Arp 220, when using L_{FIR} as the SFR indicator, the ULF greatly overestimates the whole point source population. $L_{H\alpha}$ values for this galaxy were also used to calculate the SFR of the system (Young et al. 1996; Colina et al. 2004) but, due to the very dusty nature of this object, are subject to large extinction effects, leading to greatly reduced SFRs with values as little as 0.55, which, given the merger status of this system, is unlikely to be a true measure of the SFR.

To investigate the reliability of using the L_{FIR} SFR indicator to normalize the ULF, the detected point source populations (with $L_X \leqslant 2.1 \times 10^{40} \, \text{erg s}^{-1}$) from the *Chandra* observations were used to derive SFRs from equation (5) for a number of galaxies in our sample; these values are plotted against the L_{FIR} derived SFR values in Fig. 17. Only seven of the nine systems have been included in this figure, as the ULF is only a measure of the HMXRB population, and, it is likely that the stellar populations from the two older merger remnants are dominated by LMXRBs. From Fig. 17, it can be seen that at high levels of the L_{FIR} SFR indicator, the SFR derived from equation (5) is much smaller, indicating that, in very active star-forming systems, the prediction of the point source population, when using the L_{FIR} SFR value, does not represent the observed X-ray population well.

This relationship between L_X and SFR was also investigated in Gilfanov, Grimm & Sunyaev (2004), where active systems in the *Hubble Deep Field*-North (HDF-N) were used to probe the ULF at
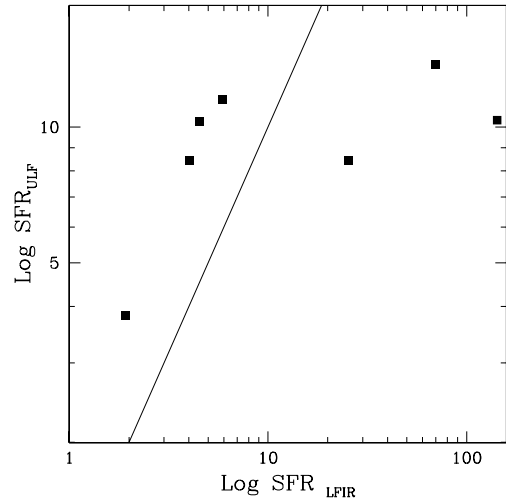

Figure 17. A plot of the SFR indicated by L_{FIR} and the SFR derived from equation (5), with the solid line indicating unity. Arp 222 and NGC 1700 have not been included in this plot as their point source populations are likely to be dominated by LMXRBs.

high values of SFR. From this work it was found that, for higher levels of star formation, the observed X-ray luminosities from these galaxies do follow the L_X–SFR relation. However, the calculated SFR for all of these systems were derived from 1.4 GHz, L_ν, SFR indicators only, not L_{FIR} SFR indicators. This suggests that the discrepancy between L_{FIR} SFR, and the observed values derived from the *Chandra* observations, is a consequence of the normalization indicator chosen, and do not arise from non-linearity of the ULF at high values of SFR.

There are a number of reasons why the SFRs inferred from the X-ray observations and L_{FIR} values might differ so greatly for systems in the most active phases. It could simply be that, for dusty, active systems such as these, L_{FIR} is a poor tracer of SFR, becoming greatly enhanced due to the large amounts of gas residing in the galaxy. This would indicate that it is the L_{FIR} SFR indicator, not the SFR from the ULF, that is incorrect. However, this explanation is unlikely, as studies have shown that, whilst $L_{H\alpha}$ and L_{UV} are susceptible to extinction caused by the presence of dust in star-forming regions, L_{FIR} does not vary with gas content, and scales well with both extinction corrected L_{UV} and radio continuum emission in dusty starbursts (Buat 1992; Buat & Xu 1996).

Alternatively, the discrepancy between the predicted and observed values could be a consequence of the age of the stellar population. If the starburst has only recently taken place, it is plausible that, whilst L_{FIR} has had enough time to become massively enhanced, the X-ray point source population has not yet evolved into HMXRBs. The consequence of this would be that the X-ray luminosity arising from the point source population is lower than the SFR, indicated by L_{FIR}, would predict. Wilson et al. (2005) recently reported on an optical study of Arp 220 which has detected two populations of young massive star clusters. The age of the youngest of these populations has been found to be 5–10 Myr, indicating that enough time has elapsed since the last starburst for HMXRBs to form ($\sim$1–10 Myr). It is therefore unlikely that a lag between L_{FIR} and L_X is the reason for the difference in the SFR values shown in Fig. 17.

Another reason that the SFR derived from equation (5) is lower than expected, when compared to the L_{FIR} SFR, could simply be that the X-ray observations are not detecting all the point sources in very active galaxies due to obscuration, and those that are being

detected have greatly reduced luminosities. To investigate this, the optical obscuration in Arp 220 (Shioya, Taniguchi & Trentham 2001) has been converted into an absorbing column density, giving $N_{\rm H} = 2.2 \times 10^{22}$ atom cm^{-2}, a value which is actually somewhat smaller than the modelled value given in Clements et al. (2002) of 3×10^{22} atom cm^{-2}. This demonstrates that the stated luminosities in Clements et al. (2002) are reliable values, and all the point sources with $L_{\rm X} \geqslant 5 \times 10^{39}$ erg s^{-1} (the stated lower luminosity point source detection threshold) should have been detected in this system.

A final explanation for the difference between the predicted and observed SFR indicators for systems close to the point of nuclear coalescence could arise from a physical change in the birth of stellar systems. These merging galaxies provide extreme examples of violent star formation, and it is therefore possible that the most recent starburst has resulted in the birth of a stellar population with a different initial mass function (IMF).

The IMF, the distribution of masses with which stars are formed, has long been a contentious issue, with a variety of different models used to explain the observed stellar populations (Larson 1986, 1998). It was initially proposed that the IMF was a universal function with a power-law form, regardless of formation time or local environment (Salpeter 1955). However, it has also been argued that the IMF varies, and was more top-heavy at earlier times (Rieke et al. 1980).

From the most recent observations it is thought that the Salpeter IMF, with a lower mass flattening between 0.5 and 1.0 M$_{\odot}$, can be considered a reasonable approximation for large regions of starburst galaxies (Elmegreen 2005), with some suggestion of small variations with environment, with denser and more massive star clusters producing more massive stars compared to intermediate-mass stars (Elmegreen 2004; Shadmehri 2004). This more top-heavy IMF has the effect of generating greater numbers of SN remnants, black holes and HMXRBs, as well as higher amounts of $L_{\rm FIR}$ per unit mass of stars formed, therefore, leading to an increase in both $L_{\rm X}$ and $L_{\rm FIR}$. However, the level of enhancement of $L_{\rm FIR}$, relative to the increase in HMXRBs formed, is dependent on the shape of the IMF.

In the galaxy systems close to the point of nuclear coalescence presented in this sample, the XRB population is dominated by HMXRBs, meaning that $L_{\rm X}$ will scale with the number of massive stars produced, whereas $L_{\rm FIR}$ will scale with the main-sequence luminosity of those stars. As the IMF flattens, $L_{\rm FIR}$ will rise more steeply, a consequence of the strong mass to luminosity dependence, $M \propto L^{3.5}$. Therefore, when using $L_{\rm FIR}$ values to derive the SFR for these system, this value will be overestimated.

If this interpretation is correct, it could explain why there appears to be a deficit of XRBs in the *Chandra* observations of the systems close to the point of coalescence. In actual fact, what is being seen here is an overestimated SFR, derived from the massively enhanced $L_{\rm FIR}$, as can be seen in Fig. 17.

5 DISCUSSION: X-RAY EVOLUTION

The first thing to note from Fig. 16 is that Arp 270, even though an early stage system, is already exhibiting enhanced star formation activity, as measured by $L_{\rm FIR}/L_K$ (see Read & Ponman 2001), compared to the typical spiral system, NGC 2403. This activity increases up to the point of nuclear coalescence, after which there is a steady drop in $L_{\rm FIR}/L_K$ until the merger-remnant systems, ~ 1 Gyr after coalescence. From this point the activity value levels off to that of a typical elliptical system.

The evolution of the X-ray luminosity is different to that of $L_{\rm FIR}/L_K$. There is initially a rise, as seen with the star formation activity, but this peaks ~ 300 Myr before coalescence takes place,

whilst $L_{\rm FIR}/L_K$ is still increasing. From this peak it drops until the young merger remnants, as is the case for $L_{\rm FIR}/L_K$. However, instead of levelling off, the X-ray luminosity once again begins to rise, with the total X-ray luminosity of the 3-Gyr system beginning to resemble that of a mature elliptical galaxy.

Both $L_{\rm X}/L_B$ and $L_{\rm X}/L_K$ broadly exhibit the same variations. One notable exception is the value of $L_{\rm X}/L_B$ for Mrk 266. This relatively small value is due the massive enhancement of L_B from this system's AGN (Risaliti & Elvis 2004), which L_K is not susceptible to, therefore indicating that L_K is a more reliable tracer of galaxy mass than L_B, and will exhibit less scatter.

The evolution of per cent $L_{\rm diff}$ also shows an increased value for Arp 270, when compared to the typical spiral system. This value then steadily rises, up to a point ~ 200 Myr prior to nuclear coalescence. This trend line then drops until the young merger-remnant systems, once again rising, with the 3-Gyr system exhibiting a similar value of per cent $L_{\rm diff}$ to that of the typical elliptical, NGC 2434.

5.1 Previous X-ray studies

In RP98 it was found that the X-ray luminosity of the sample generally followed the same patterns as the star formation activity, with the peak of $L_{\rm X}/L_B$ being coincident with nuclear coalescence. Furthermore, in the RP98 study, the sample of post-merger systems was limited, with a baseline extending out to only 1.5 Gyr after nuclear coalescence. Consequently, no rise in the X-ray luminosity of post-merger systems was observed, because, as shown in the present study, there is a strong suggestion that systems require a much greater relaxation time before they begin to exhibit properties seen in mature elliptical galaxies. This idea is further strengthened by a study of post-merger ellipticals (O'Sullivan, Forbes & Ponman 2001), where a long-term trend (~ 10 Gyr) for $L_{\rm X}/L_B$ to increase with dynamical age was found.

The reason that the peak in $L_{\rm X}$ has been found at two different merger ages in these studies could be due to the different observatories that were used. *Chandra* has greater spatial resolution than *ROSAT*, and is able to disentangle background galaxies from the target object with much greater accuracy. It is therefore possible that these objects were included in the previous *ROSAT* work as diffuse features, leading to a different peak value of $L_{\rm X}$. However, both samples include the famous merger system, the Antennae, and the system at coalescence, Arp 220, and the X-ray luminosities from both of these systems are comparable between *ROSAT* and *Chandra*. Indicating that this discrepancy does not arise from a difference between these two observatories.

Another difference between RP98 and the current work, that could account for the differing merger ages of peak $L_{\rm X}$, is the selection of systems within each study. In our sample we include two systems between the Antennae and Arp 220: Mrk 266 and NGC 3256, in RP98 there is only one, NGC 520. This system is highlighted in RP98 as being X-ray faint, not exhibiting the X-ray properties that one would expect, given its large $L_{\rm FIR}/L_K$ ratio. They suggest that this galaxy does not appear to be on the same evolutionary path as the rest of their sample and, possibly, will not evolve into an elliptical galaxy.

A recent study of NGC 520 with *Chandra* (Read 2005) has indicated that this system comprises one gas-rich and one gas-poor galaxy, not two gas-rich spirals as has been selected within this sample. This lack of gas in the second galaxy has resulted in a 'half merger' being induced in this system, and hence appears underluminous in X-rays. Therefore, it is likely that the peak X-ray luminosity was missed in the RP98 sample due to the galaxy selection. In the

present study, use of the selection criteria outlined in Section 2 has meant that only systems that are gas rich have been included, ensuring that comparable systems in the merger sequence have been selected. Consequently, the systems presented in this sample are more likely to be representative of the typical merger evolution.

5.2 The X-ray luminosity peak and the impact of galactic winds

From the X-ray luminosities of the systems within this sample it has been seen, for the first time, that both L_X/L_K and L_X/L_B peak ∼300 Myr before nuclear coalescence takes place. This result, given that the normalized SFR is still increasing at this time, is initially surprising, as one would expect the X-ray luminosity to increase with increasing L_{FIR}/L_K. However, from looking at the morphology of the hot diffuse gas, it is clear that the systems emitting very high levels of L_{FIR}/L_K are also experiencing outflows from starburst-driven winds. We propose that this relative reduction in X-ray luminosity, for these very active systems, is a consequence of these large-scale diffuse outflows.

Starburst-driven winds are responsible for the transport of gas and energy out of star-forming galaxies. The energetics of these galactic winds were investigated by Strickland & Stevens (2000), where hydrodynamical simulations were compared to the observations of the galactic wind of M82. From this work it was shown that the majority of the thermal and kinetic energy of galactic winds is in a hot volume-filling component of the gas, which is very difficult to probe due to its low emissivity, a consequence of the low density of this component.

Within our sample, the system that represents the peak X-ray luminosity is Mrk 266. In Section 3.1 the results from the *Chandra* observation of this system are presented and tentative evidence suggesting that this system is just about to experience galaxy wide diffuse outflows is found. If this interpretation is correct, it seems probable that the lower values of L_X/L_B and L_X/L_K, for NGC 3256 and Arp 220, the most active systems in this sample, are a consequence of their extensive galactic winds, which have allowed the density, and hence the emissivity, of the hot gas to drop.

5.3 Halo regeneration in low L_X systems

Another interesting result from this survey is the increase in L_X in the older merger remnants. In previous studies (e.g. RP98) post-merger systems have been found to be X-ray faint when compared to elliptical galaxies. In our study the merger sequence has been extended to include a 3-Gyr system, and, by doing so, it has been shown that these underluminous systems appear to increase in L_X as they age. Given that these merger remnants have been shown to be quiescent, this increase in L_X is not due to any starburst activity within the system. Coupling this, with the increase in per cent L_{diff}, indicates that diffuse X-ray gas is being produced, leading to the creation of X-ray haloes, as observed in mature elliptical galaxies. O'Sullivan et al. (2001) investigated the relationship between L_X/L_B and spectroscopic age in post-merger ellipticals and found that there was a long-term trend (∼10 Gyr) for L_X to increase with time. The mechanism by which the regeneration of hot gas haloes in these galaxies is explained is one in which an outflowing wind to hydrostatic halo phase is driven by a declining Type Ia SN rate. O'Sullivan et al. (2001) argue that a scenario in which gas, driven out during the starburst, infalls on to the existing halo is not the dominant mechanism in generating X-ray haloes as this mechanism would only take ∼1–2 Gyr and would therefore not produce the long-term trend they

observe. The time baseline from the sample studied in the present paper is not sufficient to allow us to discriminate between these two possibilities.

5.4 The behaviour of the X-ray point source population

From the *Chandra* observations in this study, the behaviour of the point source population during the merger process has been characterized for the first time. In Fig. 18 the total luminosity as well as its two components, the luminosity arising from the point source population (L_{src}) and the diffuse gas contribution (L_{diff}), have been normalized by L_K and plotted against star formation activity (L_{FIR}/L_K).

From this figure it can be seen that the total L_X/L_K, whilst showing a general trend of increasing with L_{FIR}/L_K, exhibits a large amount of scatter, peaking at the merger system Mrk 266, and then dropping at high values of L_{FIR}/L_K. Decomposing L_X/L_K into separate source and diffuse contributions to L_X, it can be seen that the scatter arises primarily from the diffuse component, whilst the drop in L_X/L_K at high L_{FIR}/L_K, is a consequence of both L_{diff}/L_K and L_{src}/L_K falling steeply. Using the Kendall rank coefficient, it was found that the point source component, L_{src}/L_K, shows a correlation of 2.5σ with L_{FIR}/L_K. Fitting a single power law to these data gives a logarithmic index of 0.93 ± 0.28.

However, from visual inspection of Fig. 18, a single power-law trend does not represent the behaviour adequately. At high values of L_{FIR}/L_K, the very active systems in this sample actually exhibit declining values of L_X/L_K as L_{FIR}/L_K increases. In Section 4.2, we proposed the possibility that these systems close to nuclear coalescence have a value of L_{FIR} enhanced relative to that in less extreme environments, due to a change in the IMF. Under this hypothesis, the corresponding points in Fig. 18 will have been shifted strongly to the right, which could account for the negative slope seen in all three curves at high L_{FIR}/L_K. The idea that the change in behaviour relates to L_{FIR}/L_K, rather than L_X/L_K, is attractive since, given the very different mechanisms responsible for generating the source and diffuse components of L_X (XRBs and SN-heated gas, respectively),
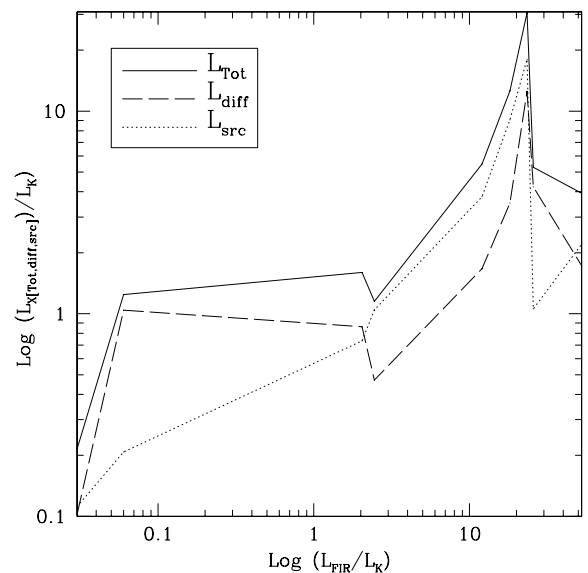

Figure 18. Plot indicating how L_X/L_K and the two components that contribute to L_X/L_K [the point source contribution (L_{src}) and the diffuse gas contribution (L_{diff})] scale with L_{FIR}/L_K.

it is hard to envisage any process which could simultaneously change the behaviour of both.

6 CONCLUSIONS

From a sample of nine interacting and merging galaxies, the evolution of X-ray emission, ranging from detached spiral pairs through to merger-remnant systems, has been investigated. As part of this survey, results from the analysis of two *Chandra* observations, Mrk 266 and Arp 222, have also been presented. Here we summarize the results from these *Chandra* observations and then draw the main conclusions from the survey.

6.1 Mrk 266 and Arp 222

(i) The luminous merger system, Mrk 266, has been shown to contain two nuclei, with X-ray luminosities of 3.47×10^{41} and 1.04×10^{41} erg s^{-1}. In addition, an area of enhanced X-ray emission has been detected between them. This is coincident with a radio source and is likely a consequence of the collision between the two discs from the progenitors. A region of diffuse emission is detected to the north of the system. It is probable that this arises from a spiral arm that has been stripped out of the system during the merger. To the south-east of the nucleus, a region of extended emission has been detected, indicating that this system could be on the verge of large-scale galactic winds breaking out. This system has the highest L_X/L_K ratio of any of the galaxies within our sample.

(ii) 15 discrete X-ray sources have been detected in Arp 222, two of which are classified as ULXs. This merger-remnant system has been shown to be X-ray faint when compared to both other systems within this sample and the typical elliptical galaxy NGC 2434. The diffuse gas of Arp 222 has been modelled with a temperature of 0.6 keV and, even though optical and CO observations are consistent with those of elliptical galaxies, the X-ray luminosity of Arp 222 does not resemble that of a mature elliptical.

6.2 The X-ray evolution of merging galaxies

(i) The most striking result from this work is the time at which L_X/L_B and L_X/L_K peak. It was previously believed that this was coincident with nuclear coalescence, but here we find the peak ∼300 Myr before this coalescence takes place. We suggest that subsequent drop in X-ray emission is a consequence of large-scale diffuse outflows breaking out of the galactic discs, reducing the hot gas density and allowing the escape of energy in kinetic form.

(ii) This study has also demonstrated that, in the systems close to the point of coalescence, L_{FIR} is massively enhanced when compared to the XRB luminosity of these systems. We suggest here that the high level of L_{FIR} result from a change in the IMF in these exceptional starbursts. With the production of more massive stars compared to intermediate-mass stars in these galaxies leading to larger values of L_{FIR} per unit mass of stars formed.

(iii) At a time ∼1 Gyr after coalescence, the merger remnants in our sample are X-ray faint when compared to typical X-ray luminosities of mature elliptical galaxies. However, we see evidence that these systems will start to resemble typical elliptical galaxies at a greater dynamical age, given the properties of the 3-Gyr system within our sample. This supports the idea that halo regeneration will take place within low L_X merger remnants. We caution that, with only one older, more relaxed, system within our sample, our conclusions on this point are necessarily tentative. To fully understand how young merger remnants evolve into typical elliptical systems, the period in which this transformation takes place needs to be studied in greater detail.

REFERENCES

Brassington N. J., Read A. M., Ponman T. J., 2005, MNRAS, 360, 801

Brown R. J. N., Forbes D. A., Kissler-Patig M., Brodie J. P., 2000, MNRAS, 317, 406

Bruzual A. G., Charlot S., 1993, ApJ, 405, 538

Buat V., 1992, A&A, 264, 444

Buat V., Xu C., 1996, A&A, 306, 61

Cappi M. et al., 2006, A&A, 446, 459

Cash W., 1979, ApJ, 228, 939

Clements D. L., McDowell J. C., Shaked S., Baker A. C., Borne K., Colina L., Lamb S. A., Mundell C., 2002, ApJ, 581, 974

Colbert E., Heckman T., Ptak A., Strickland D., Weaver K. A., 2004, ApJ, 602, 231

Colina L., Arribas S., Clements D., 2004, ApJ, 602, 181

Condon J. J., Yin Q. F., 1990, ApJ, 357, 97

Crabtree D. R., Smecker-Hane T., 1994, BAAS, 26, 1499

David L. P., Jones C., Forman W., 1992, ApJ, 388, 82

Davies R., Ward M., Sugai H., 2000, ApJ, 535, 735

de Vaucouleurs G., de Vaucouleurs A., Corwin H. G., Buta R. J., Paturel G., Fouque P., 1991, Third Reference Catalogue of Bright Galaxies, Vols 1–3, XII. Springer-Verlag, Berlin

Devereux N. A., Eales S. A., 1989, ApJ, 340, 708

Dreyer J. L. E., 1988, NGC 2000.0. Cambridge Univ. Press, Cambridge

Elmegreen B. G., 2004, MNRAS, 354, 367

Elmegreen B. G., 2005, in de Frijs R., González Delgado R. M., eds, ASSL Vol. 329, Starbursts: From 30 Doradus to Lyman Break Galaxies. Kluwer, Dordrecht, p. 57

English J., Norris R. P., Freeman K. C., Booth R. S., 2003, AJ, 125, 1134

Fabbiano G., Krauss M., Zezas A., Rots A., Neff S., 2003, ApJ, 598, 272

Fabbiano G. et al., 2004, ApJ, 605, L21

Georgakakis A., Forbes D. A., Norris R. P., 2000, MNRAS, 318, 124

Giacconi R. et al., 2001, ApJ, 551, 624

Gilfanov M., Grimm H.-J., Sunyaev R., 2004, MNRAS, 347, L57

Grimm H.-J., Gilfanov M., Sunyaev R., 2003, MNRAS, 339, 793

Heckman T. M., Dahlem M., Eales S. A., Fabbiano G., Weaver K., 1996, ApJ, 457, 616

Hernández-Toledo H. M., Puerari I., 2001, A&A, 379, 54

Hibbard J. E., Mihos J. C., 1995, AJ, 110, 140

Ishigaki T. et al., 2000, PASJ, 52, 185

Kollatschny W., Kowatsch P., 1998, A&A, 336, L21

Larson R. B., 1986, MNRAS, 218, 409

Larson R. B., 1998, MNRAS, 301, 569

Levenson N. A., Weaver K. A., Heckman T. M., Awaki H., Terashima Y., 2004, ApJ, 602, 135

Lípari S., Díaz R., Taniguchi Y., Terlevich R., Dottori H., Carranza G., 2000, AJ, 120, 645

Lira P., Ward M., Zezas A., Alonso-Herrero A., Ueno S., 2002, MNRAS, 330, 259

Liu C. T., Kennicutt R. C., 1995, ApJ, 450, 547

McDowell J. C. et al., 2003, ApJ, 591, 154

Matt G., Fabian A. C., Guainazzi M., Iwasawa K., Bassani L., Malaguti G., 2000, MNRAS, 318, 173

Mattila S., Meikle W., 2001, MNRAS, 324, 325

Mazzarella J. M., Gaume R. A., Aller H. D., Hughes P. A., 1988, ApJ, 333, 168

Mihos J. C., Hernquist L., 1996, ApJ, 464, 641

Mihos J. C., Bothun G. D., Richstone D. O., 1993, ApJ, 418, 82

Miller B. W., Whitmore B. C., Schweizer F., Fall S. M., 1997, AJ, 114, 2381

Moshir M. et al., 1990, BAAS, 22, 1325

Nolan L. A., Ponman T. J., Read A. M., Schweizer F., 2004, MNRAS, 353, 221

O'Sullivan E., Forbes D. A., Ponman T. J., 2001, MNRAS, 324, 420

Read A. M., 2003, MNRAS, 342, 715

Read A. M., 2005, MNRAS, 359, 455

Read A. M., Ponman T. J., 1998, MNRAS, 297, 143

Read A. M., Ponman T. J., 2001, MNRAS, 328, 127

Rieke G. H., Lebofsky M. J., Thompson R. I., Low F. J., Tokunaga A. T., 1980, ApJ, 238, 24

Risaliti G., Elvis M., 2004, in Barger A., ed., ASSL Vol. 308, Supermassive Black Holes in the Distant Universe. Kluwer, Dordrecht, p. 187

Risaliti G., Maiolino R., Salvati M., 1999, ApJ, 522, 157

Rosa-González D., Terlevich E., Terlevich R., 2002, MNRAS, 332, 283

Rothberg B., Joseph R. D., 2004, AJ, 128, 2098

Salpeter E. E., 1955, ApJ, 121, 161

Sanders D. B., Scoville N. Z., Young J. S., Soifer B. T., Schloerb F. P., Rice W. L., Danielson G. E., 1986, ApJ, 305, L45

Schlegel E. M., Pannuti T. G., 2003, AJ, 125, 3025

Schweizer F., 1982, ApJ, 252, 455

Seigar M. S., 2005, MNRAS, 361, L20

Shadmehri M., 2004, MNRAS, 354, 375

Shioya Y., Taniguchi Y., Trentham N., 2001, MNRAS, 321, 11

Soria R., Wu K., 2003, A&A, 410, 53

Soria R., Cropper M., Motch C., 2005, Chin. J. Astron. Astrophys., 5, 153

Statler T. S., McNamara B. R., 2002, ApJ, 581, 1032

Statler T. S., Smecker-Hane T., Cecil G. N., 1996, AJ, 111, 1512

Strickland D. K., Stevens I. R., 2000, MNRAS, 314, 511

Toomre A., 1977, in Tinsky B. M., Larson T. B., eds, Evolution of Galaxies and Stellar Populations. Yale University Observatory, New Haven, CT, p. 401

Toomre A., Toomre J., 1972, ApJ, 178, 623

Tully R. B., 1988, Nearby Galaxies Catalog. Cambridge Univ. Press, Cambridge

Wang J., Heckman T., Weaver K., 1997, ApJ, 474, 659

Wilson C. D., Harris W. E., Longden R., Scoville N. Z., 2005, ApJ, 641, 763

Young J. S., Allen L., Kenney J. D. P., Lesser A., Rownd B., 1996, AJ, 112, 1903

Zezas A., Fabbiano G., Baldi A., Schweizer F., King A. R., Ponman T. J., Rots A. H., 2006, ApJS, 166, 211

This paper has been typeset from a TeX/LaTeX file prepared by the author.